

Development of performance test system of mass-produced  
Multi-Pixel Photon Counters for a new neutrino detector  
(新型ニュートリノ検出器に用いる半導体光検出器  
MPPCの大量性能試験システムの開発)

Haruto Kikutani  
Department of Physics, The University of Tokyo

January 25, 2021

## Abstract

The T2K experiment plans to upgrade the near detector aiming at the initial observation of the  $CP$  violation in neutrino oscillation with  $3\sigma$  significance. As one of the upgrade detectors, a new neutrino target detector, named SuperFGD, is under development. The SuperFGD consists of two million scintillator cubes, with 1 cm side, each readout with wavelength shifting fibers in the three orthogonal directions. Thanks to its high granularity and three dimensional readouts, the SuperFGD is expected to realize the efficient tracking of charged particles and a full polar angle acceptance. Those performances are important for the understanding of neutrino-nucleus interaction to reduce the systematic uncertainties on neutrino oscillation measurement.

The SuperFGD uses 56,384 Multi-Pixel Photon Counters (MPPCs) as its photosensors. The performance test of all MPPCs will be conducted before installation to assure the qualities of the MPPCs. To test a large number of MPPCs in a reasonable time frame, we have been developing a test system that measures 512 MPPCs simultaneously. The gain, breakdown voltage, relative photon detection efficiency, dark noise rate, and crosstalk probability of the MPPCs will be automatically measured in the test system. In this thesis, the development and the performance of the test system are reported.

# Contents

<b>1</b>	<b>Introduction</b>	<b>3</b>
1.1	Neutrino oscillation . . . . .	3
1.2	T2K experiment . . . . .	5
1.2.1	J-PARC neutrino beam . . . . .	5
1.2.2	Detectors . . . . .	5
1.2.3	Current status and future prospects of T2K . . . . .	6
1.3	ND280 upgrade . . . . .	6
1.3.1	Weaknesses of the current ND280 . . . . .	8
1.3.2	Design of the upgrade detector . . . . .	8
1.3.3	Expected performances of the upgrade detectors . . . . .	10
1.4	Subject of this thesis . . . . .	12
<b>2</b>	<b>Multi-Pixel Photon Counter</b>	<b>14</b>
2.1	Avalanche Photodiode . . . . .	14
2.1.1	Photodiode . . . . .	14
2.1.2	Principle of avalanche multiplication . . . . .	14
2.1.3	Geiger mode . . . . .	15
2.2	Multi-Pixel Photon Counter . . . . .	16
2.2.1	Gain . . . . .	17
2.2.2	Photon detection efficiency . . . . .	18
2.2.3	Dark noise . . . . .	18
2.2.4	Optical crosstalk . . . . .	18
2.3	MPPC used for SuperFGD . . . . .	19
2.3.1	Specification . . . . .	19
2.3.2	MPPC-PCB . . . . .	19
2.3.3	Production of MPPC . . . . .	20
2.4	Requirements for MPPCs used for SuperFGD . . . . .	21
2.4.1	Requirements for operation voltage . . . . .	21
2.4.2	Requirements for gain and PDE . . . . .	21
2.4.3	Requirements for dark noise rate and crosstalk probability . . . . .	22
2.4.4	Summary . . . . .	24
<b>3</b>	<b>Development of MPPC performance test system</b>	<b>25</b>
3.1	Purpose of the performance test . . . . .	25
3.2	Measurement items and requirements for the test system . . . . .	25
3.3	Design of the test system . . . . .	26
3.3.1	Overview . . . . .	26

3.3.2	NIM EASIROC module . . . . .	27
3.3.3	Light source . . . . .	29
3.3.4	Reference MPPC . . . . .	29
3.3.5	Measurement box . . . . .	29
3.3.6	Readout cable and interface board . . . . .	32
3.3.7	Thermostatic chamber . . . . .	32
3.4	Measurement method . . . . .	32
3.4.1	Configuration of EASIROC . . . . .	32
3.4.2	DAQ mode . . . . .	39
3.4.3	Measurement flow . . . . .	39
3.5	Analysis method . . . . .	40
3.5.1	Gain . . . . .	40
3.5.2	Operation voltage . . . . .	40
3.5.3	Breakdown voltage . . . . .	40
3.5.4	Relative PDE . . . . .	42
3.5.5	Dark noise rate . . . . .	42
3.5.6	Crosstalk probability . . . . .	44
<b>4</b>	<b>Performance of the test system</b>	<b>45</b>
4.1	Light uniformity and stability . . . . .	45
4.1.1	Light uniformity . . . . .	45
4.1.2	Light stability . . . . .	47
4.2	Stability of measurement . . . . .	50
4.2.1	Gain . . . . .	50
4.2.2	Operation voltage . . . . .	50
4.2.3	Breakdown voltage . . . . .	52
4.2.4	Relative PDE . . . . .	52
4.2.5	Dark noise rate . . . . .	53
4.2.6	Crosstalk probability . . . . .	53
4.2.7	Summary . . . . .	54
4.3	Module dependence of measurement . . . . .	54
4.3.1	Gain . . . . .	54
4.3.2	Operation voltage . . . . .	55
4.3.3	Breakdown voltage . . . . .	55
4.3.4	Relative PDE . . . . .	55
4.3.5	Dark noise rate . . . . .	56
4.3.6	Crosstalk probability . . . . .	56
4.3.7	Summary . . . . .	58
4.4	Systematic uncertainties of measurement . . . . .	58
<b>5</b>	<b>Summary and future prospects</b>	<b>60</b>
5.1	Summary . . . . .	60
5.2	Future prospects . . . . .	60
5.2.1	Differences due to light sources and measurement boxes . . . . .	60
5.2.2	Adjustment of threshold level for each MPPC-PCB . . . . .	61
5.2.3	Multiple operation of EASIROCs . . . . .	61
5.2.4	Performance test of the MPPCs used for SuperFGD . . . . .	61
<b>A</b>	<b>Measurement results of an MPPC-PCB by eight EASIROCs</b>	<b>63</b>

# Chapter 1

## Introduction

### 1.1 Neutrino oscillation

The Standard Model of particle physics describes almost all of the experiments that have been performed so far and is considered as one of the great achievements of physics. However, there are many mysteries that can not be understood in the framework of the Standard Model. The problem of matter-antimatter asymmetry, why the universe is composed of matter and there is almost no antimatter, is one of such mysteries. According to the Sakharov conditions [1], the  $CP$  (charge-conjugation and parity-reversal) violation in fundamental particles is necessary to explain the observed asymmetry of matter and antimatter. Because the  $CP$  violation in leptons is considered to generate the asymmetry through a process called leptogenesis [2], it is important to study the  $CP$  violation in leptons. The  $CP$  violation in leptons can be studied by comparing neutrino oscillation probabilities of neutrino and antineutrino.

Neutrino is one of the elementary particles and classified into neutral leptons in the Standard Model. There exist three types or flavors of neutrinos, electron neutrino ( $\nu_e$ ), muon neutrino ( $\nu_\mu$ ), and tau neutrino ( $\nu_\tau$ ). Each neutrino is coupled to the corresponding charged lepton in the charged current process of weak interaction. For each neutrino, there also exists a corresponding antiparticle, called an antineutrino.

Neutrino oscillation is a quantum mechanical phenomenon in which a flavor of neutrinos changes during their travel. Neutrino oscillation was firstly observed by the Super-Kamiokande experiment [3] and has been firmly established by multiple experiments.

Neutrino oscillation occurs when neutrinos have non degenerate masses. Let  $|\nu_i\rangle$  ( $i = 1, 2, 3$ ) be mass eigenstate of neutrinos that has mass of  $m_i$ . The neutrino flavor eigenstate  $|\nu_\alpha\rangle$  ( $\alpha = e, \mu, \tau$ ) can be expressed as superposition of the mass eigenstates:

$$|\nu_\alpha\rangle = \sum_i U_{\alpha i}^* |\nu_i\rangle, \quad (1.1)$$

where  $U$  is a  $3 \times 3$  unitary matrix, called the Pontecorvo-Maki-Nakagawa-Sakata (PMNS) matrix [4, 5]. The matrix can be parameterized in terms of the three mixing angles,  $\theta_{12}$ ,  $\theta_{23}$ , and  $\theta_{13}$ , and one complex phase  $\delta_{CP}$  as

$$U = \begin{pmatrix} 1 & 0 & 0 \\ 0 & c_{23} & s_{23} \\ 0 & -s_{23} & c_{23} \end{pmatrix} \begin{pmatrix} c_{13} & 0 & s_{13}e^{-i\delta_{CP}} \\ 0 & 1 & 0 \\ -s_{13}e^{i\delta_{CP}} & 0 & c_{13} \end{pmatrix} \begin{pmatrix} c_{12} & s_{12} & 0 \\ -s_{12} & c_{12} & 0 \\ 0 & 0 & 1 \end{pmatrix}, \quad (1.2)$$

where  $c_{ij} = \cos \theta_{ij}$  and  $s_{ij} = \sin \theta_{ij}$  ( $i, j = 1, 2, 3$ ).

The probability of  $\nu_\alpha \rightarrow \nu_\beta$  oscillation in vacuum is calculated as

$$P(\nu_\alpha \rightarrow \nu_\beta) = \delta_{\alpha\beta} - 4 \sum_{i < j} \text{Re}[U_{\alpha i} U_{\beta i}^* U_{\alpha j} U_{\beta j}] \sin^2 \left( \frac{\Delta m_{ij}^2 L}{4E} \right) + 2 \sum_{i < j} \text{Im}[U_{\alpha i} U_{\beta i}^* U_{\alpha j} U_{\beta j}] \sin^2 \left( \frac{\Delta m_{ij}^2 L}{2E} \right), \quad (1.3)$$

where  $E$ ,  $L$ , and  $\Delta m_{ij}^2 = m_i^2 - m_j^2$  is the energy of the neutrino, the distance that the neutrino travels, and the squared mass difference of neutrinos, respectively.

For accelerator-based neutrino oscillation experiments,  $\nu_\mu \rightarrow \nu_\mu$  and  $\nu_\mu \rightarrow \nu_e$  oscillation probability are mainly measured. Because  $\Delta m_{21}^2$  is much smaller than  $|\Delta m_{32}^2|$ , the dominant term of  $\nu_\mu$  survival probability is written as

$$P(\nu_\mu \rightarrow \nu_\mu) \simeq 1 - \sin^2 2\theta_{23} \sin^2 \left( \frac{1.27 \Delta m_{32}^2 [\text{eV}^2] L [\text{km}]}{E [\text{GeV}]} \right). \quad (1.4)$$

From this channel,  $\sin^2 2\theta_{23}$  and the absolute value of  $\Delta m_{32}^2$  can be measured. The  $\nu_e$  appearance probability is dominated by

$$P(\nu_\mu \rightarrow \nu_e) \simeq \sin^2 2\theta_{13} \sin^2 \theta_{23} \sin^2 \left( \frac{1.27 \Delta m_{32}^2 [\text{eV}^2] L [\text{km}]}{E [\text{GeV}]} \right). \quad (1.5)$$

From this channel,  $\sin^2 2\theta_{13}$  can be measured.

It is possible to study the  $CP$  violation in neutrino oscillation by comparing the appearance probability of  $\nu_e$  and  $\bar{\nu}_e$ . The antineutrino oscillation probability is obtained by changing  $U$  to  $U^*$  in equation (1.3). Then the difference of the oscillation probability between  $\nu_\mu \rightarrow \nu_e$  and  $\bar{\nu}_\mu \rightarrow \bar{\nu}_e$ ,  $\Delta P = P(\nu_\mu \rightarrow \nu_e) - P(\bar{\nu}_\mu \rightarrow \bar{\nu}_e)$ , is written as

$$\Delta P = -2 \cos \theta_{13} \sin 2\theta_{12} \sin 2\theta_{13} \sin 2\theta_{23} \sin \delta_{CP} \times \sin^2 \left( \frac{\Delta m_{32}^2 L}{4E} \right) \sin^2 \left( \frac{\Delta m_{31}^2 L}{4E} \right) \sin^2 \left( \frac{\Delta m_{21}^2 L}{4E} \right). \quad (1.6)$$

Because all the mixing angles and the squared mass differences are measured as nonzero, the requirement for the  $CP$  violation in the PMNS framework is

$$\sin \delta_{CP} \neq 0 \quad \therefore \delta_{CP} \neq 0, \pi. \quad (1.7)$$

The search for the  $CP$  violation in lepton sector is the most important topic for long-baseline neutrino oscillation experiments.

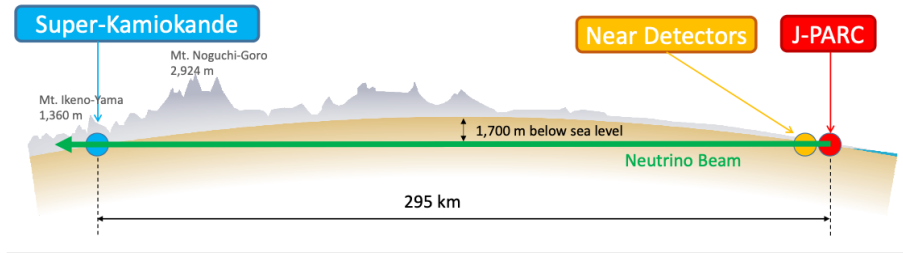


Figure 1.1: The overview of the T2K experiment.

## 1.2 T2K experiment

The T2K (Tokai to Kamioka) experiment is a long-baseline neutrino oscillation experiment. An intense muon neutrino beam is produced in Japan Proton Accelerator Research Complex (J-PARC) in Tokai and measured by several near detectors and a far detector (Super-Kamiokande). Figure 1.1 shows an overview of the T2K experiment. The main purpose of T2K is precise measurement of oscillation parameters  $\theta_{23}$ ,  $\theta_{13}$ ,  $\Delta m_{32}^2$  and the search for the  $CP$  violation in lepton sector.

### 1.2.1 J-PARC neutrino beam

The J-PARC main ring provides a 30 GeV proton beam that strikes a graphite target to produce secondary hadrons such as pions. The secondary hadrons are then focused and selected by charge with a system of magnetic horns. The hadrons decay in a 96-m-long decay volume, producing an intense muon neutrino beam:

$$\pi^+ \rightarrow \mu^+ + \nu_\mu, \quad (1.8)$$

$$\pi^- \rightarrow \mu^- + \bar{\nu}_\mu. \quad (1.9)$$

A beam predominantly composed of neutrinos or antineutrinos can be produced by choosing the polarity of the horn current.

T2K adopts the so-called off-axis method to generate a narrow-band neutrino beam. The beam axis is directed  $2.5^\circ$  away from the far detector and the flux is peaked at an energy of 600 MeV, where the effect of neutrino oscillation is maximum for a baseline of 295 km as shown in Figure 1.2.

### 1.2.2 Detectors

#### ND280

A near detector, ND280 is placed at 280 m downstream of the production target. The purpose of the ND280 is to reduce the uncertainties on neutrino flux and neutrino interaction models by measuring the neutrino interaction rates before oscillation. The ND280 is composed of a set of subdetectors, placed in a 0.2 T magnet field as shown in Figure 1.3. A tracker region of the ND280 consists of two fine-grained detectors (FGDs) interleaving three time projection chambers (TPCs). The FGDs are mainly composed of plastic scintillator bars with dimensions of  $1 \text{ cm} \times 1 \text{ cm} \times 184 \text{ cm}$ , and provide target mass for neutrino interactions.

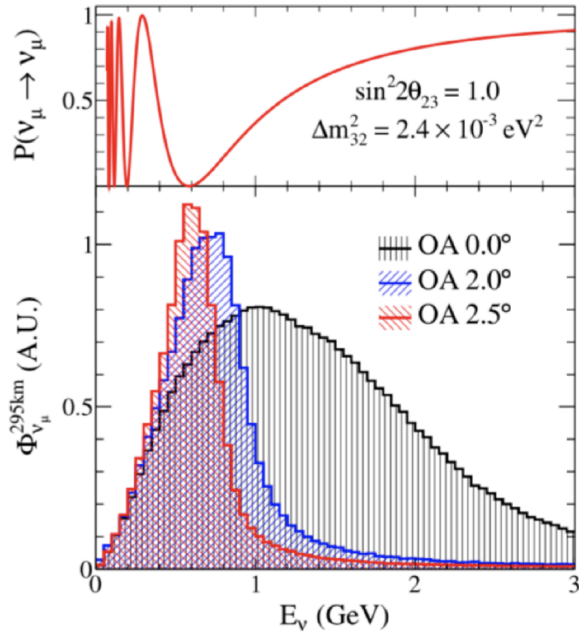


Figure 1.2: The oscillation probability of muon neutrino as a function of energy (top) and the neutrino fluxes for different off-axis angles [6].

### Super-Kamiokande

The far detector, Super-Kamiokande (SK), is a 50 kt pure water Cherenkov detector, located in the Kamioka Observatory. The water tank is covered with a large number of 20-inch photomultiplier tubes (PMTs). SK observes neutrino interactions with  $4\pi$  angular acceptance by measuring Cherenkov lights emitted by charged particles produced in neutrino interactions.

#### 1.2.3 Current status and future prospects of T2K

Since the start of the physics run in 2010, the T2K experiment has accumulated data. The accumulated protons on target (POT) from Jan 2010 to Feb 2020 is shown in Figure 1.5. The recent result with  $3.13 \times 10^{21}$  POT indicates the  $CP$  violation in lepton sector with 95% C.L. [9]. To observe the  $CP$  violation with  $3\sigma$  significance, T2K plans to accumulate  $10 \times 10^{21}$  POT until 2026. Due to the increase of statistics, it will become more important to reduce systematic uncertainties by understanding the neutrino flux and interaction model more precisely.

### 1.3 ND280 upgrade

The T2K experiment plans to upgrade the near detector ND280 to reduce systematic uncertainties. While the present configuration of ND280 leads to systematic errors of the order of 6%, the goal of the upgrade is to bring it down to 4% level. The project aims to improve the performance of ND280 by adding a new highly granular scintillator detector (SuperFGD) and two high-angle time projection chambers (HA-TPC). These detectors achieve higher granularity

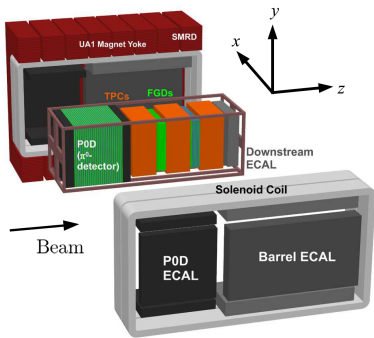


Figure 1.3: The ND280 detectors [7].

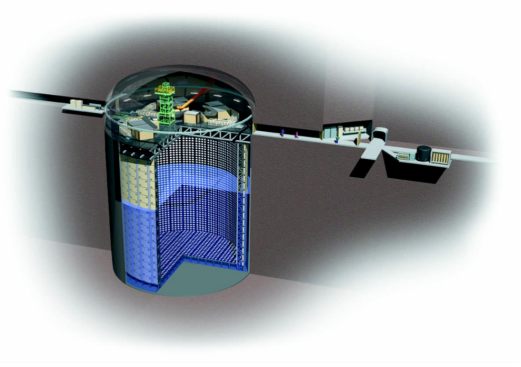


Figure 1.4: The Super-Kamiokande detector [8].

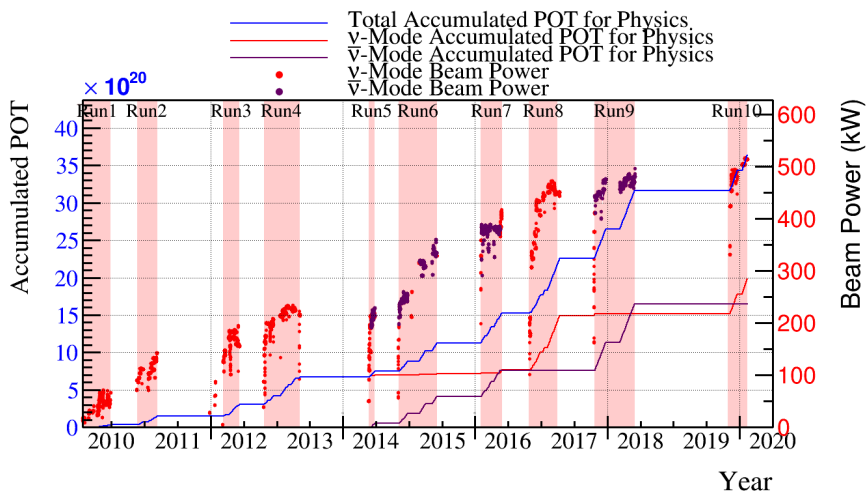


Figure 1.5: Accumulated POT from Jan 2010 to Feb 2020.

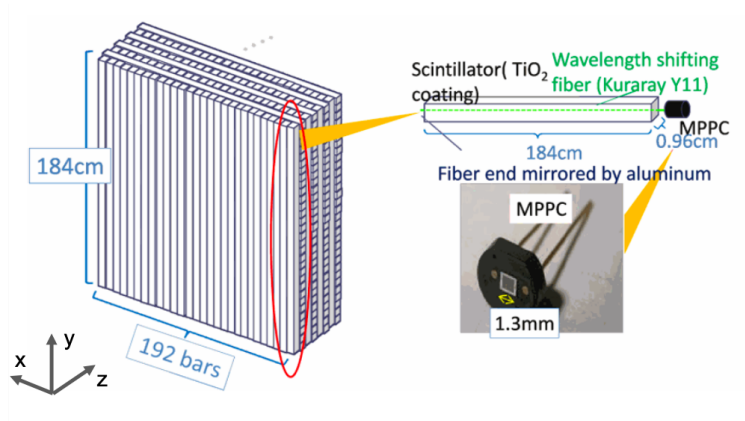


Figure 1.6: The structure of an FGD [10].

and larger angular acceptance and reduce uncertainties on the neutrino interaction model. The upgrade detectors will be installed in 2022.

### 1.3.1 Weaknesses of the current ND280

As shown in Figure 1.3, the tracker region of the ND280 consists of two FGDs interleaving three TPCs. Figure 1.6 shows the structure of an FGD. An FGD is composed of planes of scintillator bars ( $1\text{ cm} \times 1\text{ cm} \times 184\text{ cm}$ ) which are oriented in either  $x$  or  $y$  direction, perpendicular to the beam direction ( $z$  direction). Scintillation light emitted in a bar is read out along the bar by a wavelength-shifting (WLS) fiber and is detected by Multi-Pixel Photon Counter (MPPC). FGD provides projections of charged particle trajectories onto  $xz$  and  $yz$  planes.

One of the limitations of the current ND280 is low detection efficiency for charged particles with large scattering angles with respect to the beam direction. One reason is that the TPCs do not cover large angle direction, and the other reason is that the track can not be reconstructed in FGD when the trajectory of the particle is along the scintillator bar as schematically shown in Figure 1.7. Because the efficiency is uniform with respect to the beam direction at SK, the difference causes uncertainties on the predicted event rates at SK.

Another weakness is low detection efficiency for low momentum particles such as protons. For example, a proton with  $300\text{ MeV}/c$  momentum has a range of 2-3 cm. However, such a short track generates only one or two hits in each readout plane and can not be reconstructed. Therefore, to reconstruct a proton in FGD, at least a range of 4-5 cm which corresponds to  $\sim 500\text{ MeV}/c$  momentum is needed. Because the reconstruction of low momentum protons is important to understand neutrino-nucleus interactions, it is a problem.

### 1.3.2 Design of the upgrade detector

The upgrade detectors are designed to solve the problems of the current ND280. The upgrade detector will be installed in the upstream part of the current detector as shown in Figure 1.8. In the upstream part, a new highly granular scintillator detector, SuperFGD is installed as a neutrino target. Two TPCs, called High-Angle TPCs, are placed above and below SuperFGD. These three detectors form approximately a cube with 2-m-long sides. The downstream part of ND280, which consists of two FGDs and three TPCs remains unchanged. These detectors are installed inside a magnet which provides a 0.2 T magnetic field.

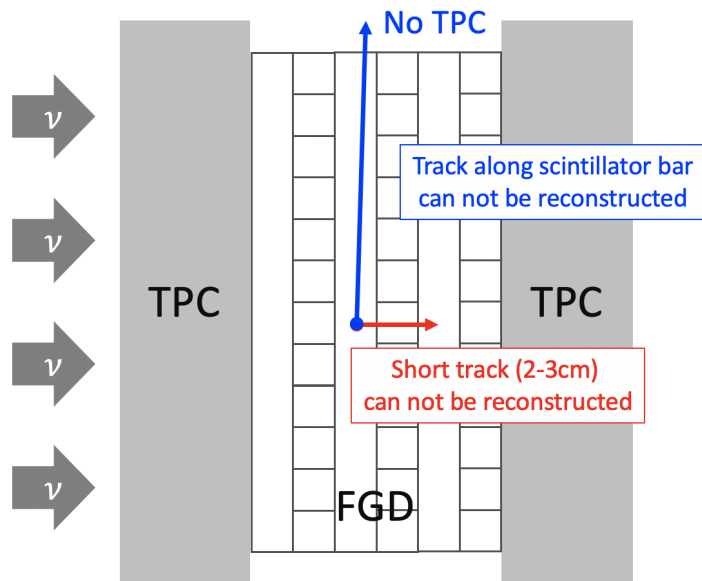


Figure 1.7: The difficult cases of the reconstruction in the current ND280.

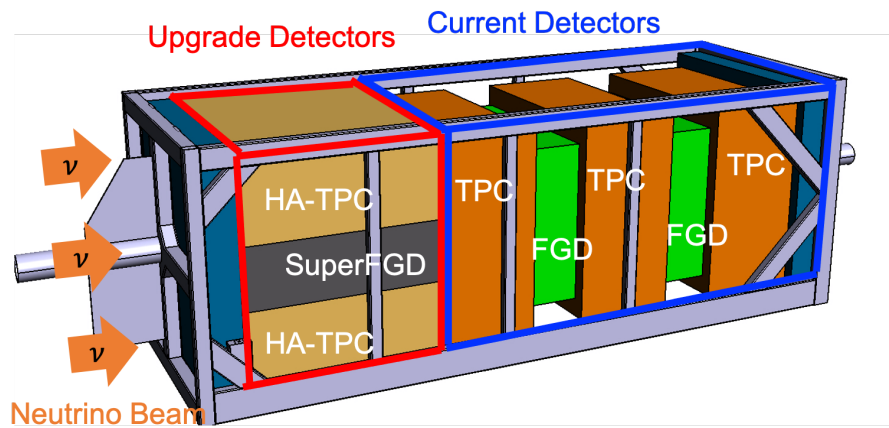


Figure 1.8: The design of the ND280 upgrade detector [11].

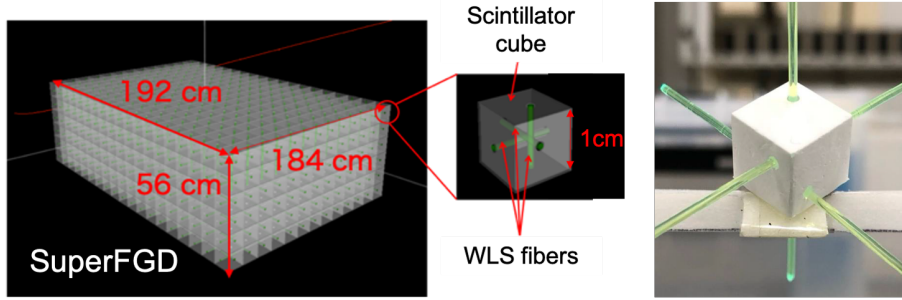


Figure 1.9: Left : the schematic view of SuperFGD [11]. Right : a scintillator cube with three WLS fibers inserted.

### SuperFGD

SuperFGD consists of  $192 \times 184 \times 56$  plastic scintillator cubes, with 1 cm side as shown in Figure 1.9. Each scintillator cube is covered with a reflecting layer to be optically separated from each other. Each cube also has three cylindrical through holes with 1.5 mm diameters in  $x$ ,  $y$ , and  $z$  directions, where WLS fibers are inserted. Scintillation light emitted along the trajectory of a charged particle produced in a neutrino interaction is read out along three orthogonal directions by the WLS fibers. One end of each WLS fiber is instrumented with an MPPC. The total number of readout channels is 56,384. SuperFGD provides projections of charged particle trajectories onto three planes.

### High-Angle TPC

High-Angle TPC consists of a field cage filled with Ar-based gas. The electrons released in the ionization of the gas by a charged particle are drifted to the anode of the field cage and read out by Micromegas detectors. TPC provides a three dimensional reconstruction of charged particles. Thanks to the existence of the magnetic field, TPC measures charge and momentum of a charged particle. By combining  $dE/dx$  with momentum measurement, TPC is also capable of particle identification.

### 1.3.3 Expected performances of the upgrade detectors

One of the expected performances of the upgrade detectors is larger angular acceptance. The charged particles scattered at a large angle can be reconstructed by the High-Angle TPCs and also in SuperFGD thanks to its isotropic structure as schematically shown in Figure 1.10. Figure 1.11 shows a simulation result of the selection efficiency of muon as a function of the muon polar angle with respect to the beam direction. The upgrade configuration clearly improves the angular acceptance for high-angle muons thanks to the HA-TPCs and SuperFGD.

Another expected performance of SuperFGD is lower momentum threshold for protons. While a proton with 300 MeV/ $c$  momentum can not be reconstructed in FGD, a track of 2-3 cm generates about two or three hits in three readout planes in SuperFGD and it can be reconstructed. Figure 1.12 shows a simulation result of reconstruction efficiency for protons stopping in SuperFGD. A proton with 300 MeV/ $c$  momentum can be reconstructed in SuperFGD. This performance is important for understanding neutrino-nucleus interaction precisely and reducing systematic uncertainties for predicted event rates at SK.

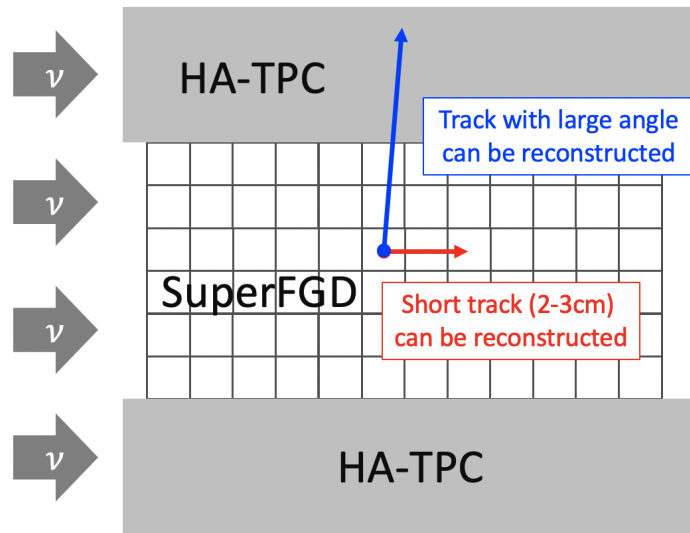


Figure 1.10: The advantage of the upgrade detectors in the reconstruction of particles with high angle and low momentum.

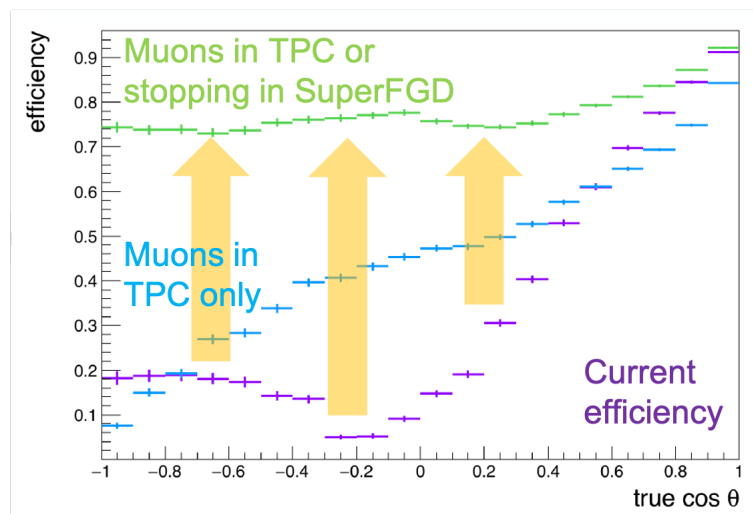


Figure 1.11: The selection efficiency for muon as a function of the muon polar angle [12]. The purple line shows the efficiency for the current ND280. The blue and green lines show the efficiency for the upgrade configuration. The blue one shows the efficiency for events in which a muon is reconstructed in a TPC. The green one shows the efficiency for events in which a muon stops and is reconstructed in SuperFGD in addition to the events in TPC.

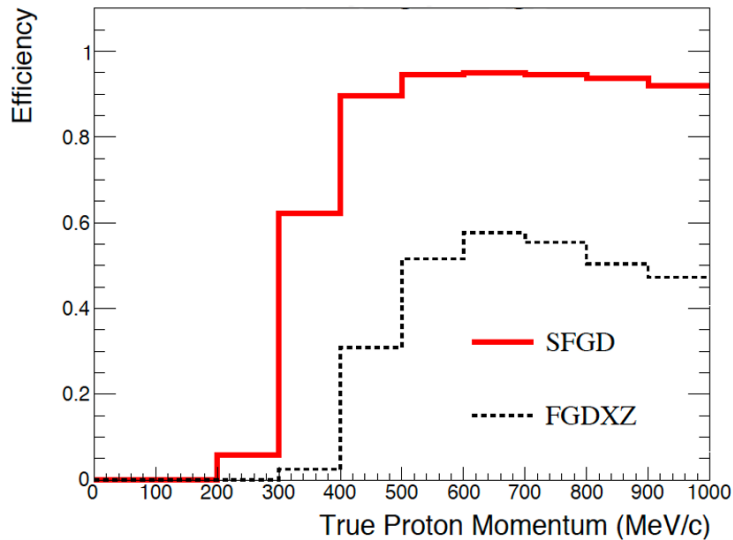


Figure 1.12: Track reconstruction efficiency for protons stopping in SuperFGD (red line) and FGD (black dashed line) [12].

The SuperFGD particle identification performance is also important especially for the particles which do not enter a TPC. The performance was studied in a beam test of a prototype of SuperFGD at CERN in 2018 [13]. Figure 1.13 shows the average energy deposit per unit length for a sample of a mix of muons and pions and a sample of protons. The muon/pion and the proton are clearly distinguishable. The capability of electron gamma separation is also being studied. It is important to separate the electron neutrino events from the background events caused by converted gammas.

## 1.4 Subject of this thesis

As presented above, we adopt MPPC as the photosensors for SuperFGD. The total number of channels is 56,384 and it is one of the largest numbers of MPPCs used in a single detector. The stable and uniform operation of all MPPCs is important for the good performance of SuperFGD. In order to assure the performance of the MPPCs, we test all MPPCs before installation to SuperFGD. To test a large number of MPPCs in a reasonable time frame, we have been developing a test system that can measure 512 MPPCs simultaneously.

In this thesis, the performance of MPPC used in SuperFGD and the development of the performance test system are reported. Chapter 2 describes the operation principle of MPPC and the details of MPPC used in SuperFGD. The design and the measurement method of the performance test system are presented in Chapter 3. Chapter 4 describes the performance of the test system. Finally, summary and future prospects are presented in Chapter 5.

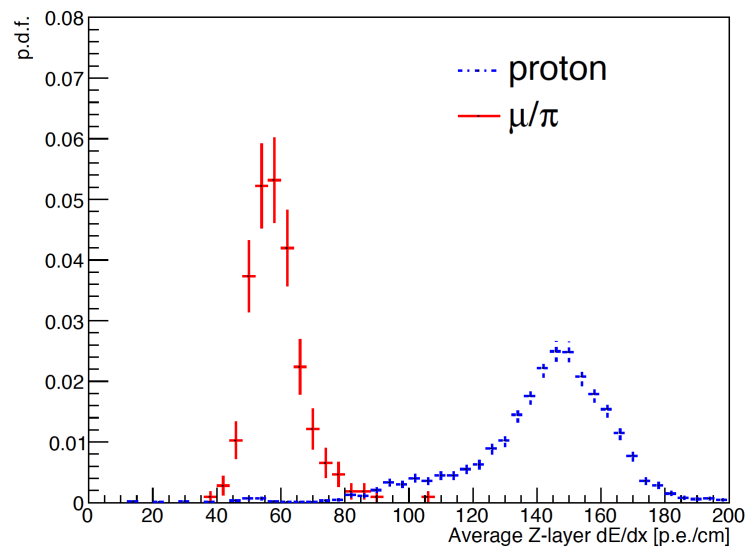


Figure 1.13: Average energy deposit per unit length for a sample of a mix of muons and pions (red) and a sample of protons (blue) [13].

## Chapter 2

# Multi-Pixel Photon Counter

The Multi-Pixel Photon Counter (MPPC), developed by Hamamatsu Photonics K.K., is one of the devices called silicon photomultipliers (SiPM) [14]. It is a photon-counting device using multiple avalanche photodiode (APD) pixels operating in the Geiger mode. So far the MPPC has been used for T2K near detectors with good performance and will be used as photosensors of SuperFGD. In this chapter, an operation principle and features of MPPC and the details of the MPPC used for SuperFGD are presented.

### 2.1 Avalanche Photodiode

As described above, MPPC consists of multiple APD pixels. The operation principle of photodiode and APD is presented in this section.

#### 2.1.1 Photodiode

A photodiode is a photosensor that generates a current when it is illuminated by light. Figure 2.1(a) shows a schematic cross section of a photodiode. A photodiode has a P-layer and an N-layer and they form a PN junction that operates as a photoelectric converter. The intrinsic region at the junction between the P-layer and the N-layer is known as the depletion layer. Because the junction makes the N-layer positive and the P-layer negative, an electric field from N-layer to P-layer is created in the depletion layer.

When a photodiode is illuminated by light and if the light energy is greater than the band gap energy, the valence band electrons are excited to the conduction band and leave holes in their place in the valence band as described in Figure 2.1(b). In the depletion layer, the electric field accelerates these electrons toward the N-layer and the holes toward the P-layer. These electrons and holes, which are also called carriers, generate an electrical current. However, because a normal photodiode does not have a function to multiply the current, it is difficult to detect a weak light such as a few photons.

#### 2.1.2 Principle of avalanche multiplication

The avalanche photodiode (APD) is a photodiode that can internally multiply photocurrent by a mechanism called avalanche multiplication. Figure 2.2 shows the schematic diagram of avalanche multiplication. The mechanism by which carriers are generated inside an APD is the same as in a photodiode. A reverse bias voltage applied to an APD creates an electric field

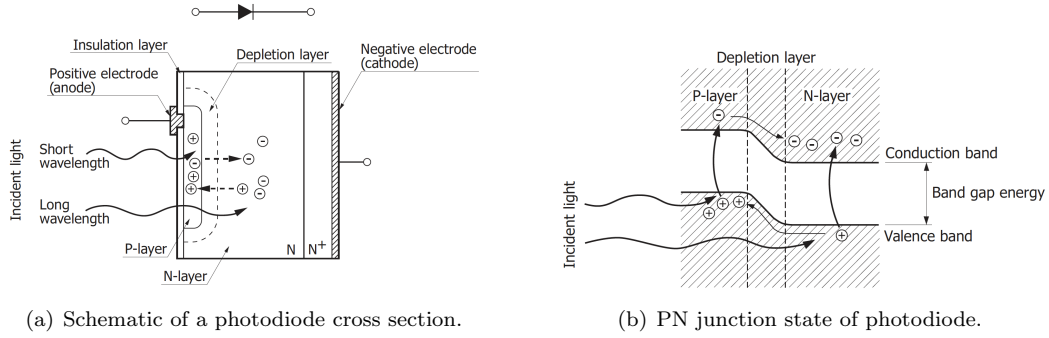


Figure 2.1: The operation principle of photodiode [15].

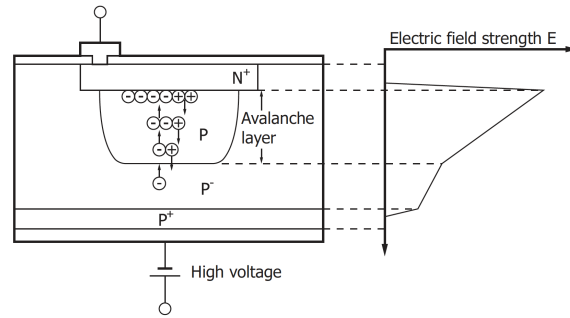


Figure 2.2: Schematic diagram of avalanche multiplication [15].

across the PN junction. It causes the electrons to drift toward the N-layer and the holes to drift toward the P-layer. As the electric field becomes stronger, the drift speed of these carriers increases. However, when the electric field reaches a certain level, the carriers are more likely to collide with the crystal lattice and create new electron-hole pairs. This phenomenon is called ionization. These electron-hole pairs then create additional electron-hole pairs, which generate a chain reaction of ionization that is called avalanche multiplication.

### 2.1.3 Geiger mode

The gain of APD depends on the electric field across the PN junction. In the normal operation range where the applied bias voltage is lower than the breakdown voltage, the gain increases as the bias voltage increases and the photocurrent increases as the number of detected photons increases. The gain in the normal mode is  $10 \sim 100$ , thus it is difficult to detect one photon signal. As the bias voltage increases, the APD eventually reaches the breakdown voltage and operates in the Geiger mode. The gain is about  $10^5 \sim 10^6$  in the Geiger mode and the photocurrent is saturated to be independent of the number of detected photons.

The Geiger mode allows obtaining a large output even when detecting a single photon. Once the Geiger discharge begins, it continues as long as the electric field in the APD is maintained. To halt the Geiger discharge and detect the next photon, a so-called quenching resistor is connected in series with the APD as shown in Figure 2.3(a). Figure 2.3(b) shows the basic operation process of a combination of the APD operating in the Geiger mode and the quenching resistor. When

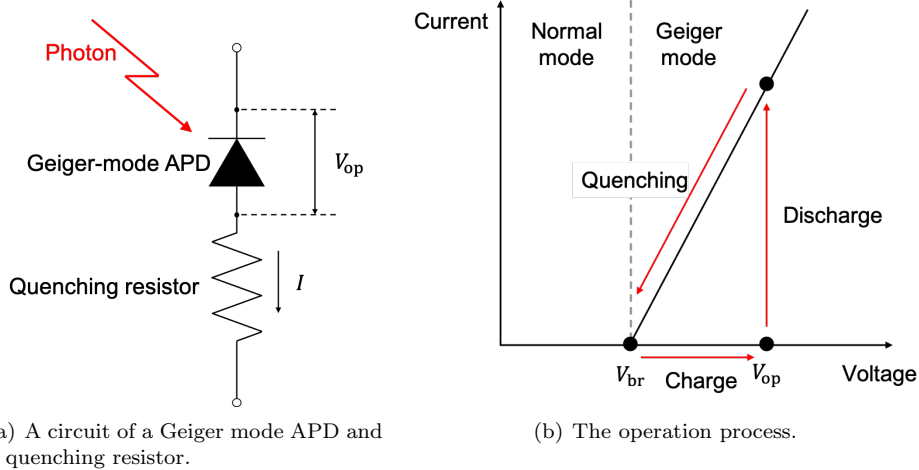


Figure 2.3: The operation process of a combination of the Geiger mode APD and the quenching resistor.

	MPPC	PMT
Gain	$10^5 \sim 10^6$	$10^6 \sim 10^7$
Operation voltage	50 ~ 80 V	1 ~ 2 kV
Active area	$\sim 1 \text{ mm}^2$	10 ~ 1000 $\text{cm}^2$
Dark count	$\sim 100 \text{ kHz}$	$\sim 1 \text{ kHz}$
PDE ( $\lambda \sim 400 \text{ nm}$ )	20 ~ 50%	20 ~ 30%
Use in magnetic field	Yes	No

Table 2.1: Comparison of photo sensors.

the APD with the bias voltage applied at the operation voltage ( $V_{op}$ ) detects photons, the Geiger discharge begins and generates an electric current. The quenching resistor reduces the operating voltage of the APD when the Geiger discharge flows in the resistor. When the operating voltage decreases to the breakdown voltage ( $V_{br}$ ), the avalanche multiplication calms down. When the current stops, the APD begins to charge again and becomes to be able to detect the next photon.

## 2.2 Multi-Pixel Photon Counter

The multi-pixel photon counter (MPPC), which is developed by Hamamatsu Photonics, is one of the devices called silicon photomultiplier. It is a photon-counting device using multiple APD pixels operated in the Geiger mode. The main features of the MPPC compared to those of the photomultiplier tube (PMT) are summarized in Table 2.1. The MPPC has features such as high gain and high photon detection efficiency compatible to a PMT and operates at a low voltage. The small size of the MPPC enables us to use it in small spaces and it can also be used in a magnetic field. On the other hand, the MPPC has a relatively high dark noise rate and some features such as gain and dark noise rate are affected by temperature.

Figure 2.4(a) shows a schematic view of an MPPC. The basic element (one pixel) of an MPPC is a combination of a Geiger mode APD and a quenching resistor. A large number of these pixels are electrically connected and arranged in a 2D plane. Each pixel in the MPPC outputs a pulse

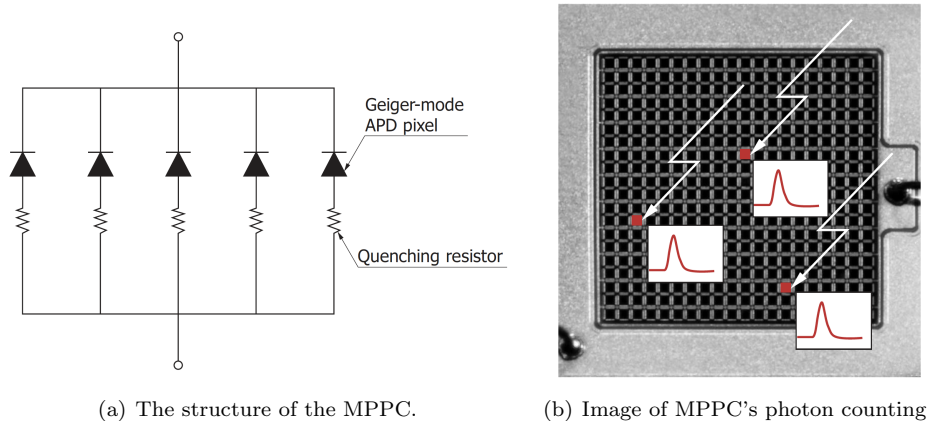


Figure 2.4: The operating principle of the MPPC [15].

at the same amplitude when it detects a photon. Pulses generated by multiple pixels are output as the sum of those pulses. Therefore, the MPPC can count the number of detected photons by measuring the amplitude of the output signal or the amount of generated charge as described in Figure 2.4(b). When the MPPC detects  $n$  photons, the output is called  $n$  photoelectron (p.e.) signal.

In the following sections, the basic properties of MPPC such as gain, PDE, dark noise rate, and optical crosstalk are described.

### 2.2.1 Gain

The MPPC gain  $M$  as a multiplication factor is defined as

$$M = \frac{Q}{e}, \quad (2.1)$$

where  $Q$  is output charge of the MPPC when one pixel detects one photon and  $e = 1.602 \times 10^{-19}$  C is the elementary charge. The output charge depends on the applied bias voltage  $V_{\text{bias}}$  and breakdown voltage  $V_{\text{br}}$  and it is expressed by the following equation

$$Q = C(V_{\text{bias}} - V_{\text{br}}) = CV_{\text{over}}, \quad (2.2)$$

where  $C$  is the capacitance of one pixel, and  $V_{\text{over}} = V_{\text{bias}} - V_{\text{br}}$  is called overvoltage. The gain increases linearly as the overvoltage increases.

It is known that the breakdown voltage of an MPPC depends on its temperature. As the temperature rises, the crystal lattice vibrations become larger. This increases the probability that carriers may collide with the vibrating crystal before it is accelerated to obtain enough energy to ionize other carriers. It decreases the probability of the Geiger discharge. Therefore, at high temperatures, the high bias voltage is needed to make the MPPC reach the breakdown voltage. To keep the gain constant, the bias voltage must be adjusted to match the temperature or the element temperature must be kept stable. The temperature dependence of the breakdown voltage is typically about 50 mV/degree.

## 2.2.2 Photon detection efficiency

The photon detection efficiency (PDE) is defined as a ratio of the number of detected photons to the number of incident photons:

$$\text{PDE} = \frac{\text{Number of detected photons}}{\text{Number of incident photons}}. \quad (2.3)$$

The PDE can be expressed by the product of a fill factor, quantum efficiency (QE) and avalanche probability:

$$\text{PDE} = \text{Fill Factor} \times \text{QE} \times \text{Avalanche probability}. \quad (2.4)$$

The fill factor is the ratio of the light detectable area to the entire pixel area of an MPPC. The MPPC photosensitive area contains sections such as the inter-pixel wiring that cannot detect light, so some photons incident on the photosensitive area are not detected. Generally, when the pixel size is smaller, the fill factor is lower.

The quantum efficiency is defined as the probability that carriers will be generated by light incident on a pixel. It depends on the wavelength of detected photons.

The avalanche probability is the probability that the carriers cause avalanche multiplication. The PDE increases as applied overvoltage increases due to the overvoltage dependence of the avalanche probability.

## 2.2.3 Dark noise

In the MPPC operation, pulses are produced not only by incident photons but also by thermally-excited carriers. The pulses produced by the thermal excitation is called the dark noise. The dark noise is observed along with the signal pulses and causes detection errors. Thermally-excited carriers are also multiplied to a constant signal level (1 p.e.). These dark noises are indistinguishable from photon-generated pulses.

The number of dark noises per second is called the dark noise rate. The dark noise rate is measured by counting the number of pulses that exceed a threshold of 0.5 p.e. signal level, without incident photons.

Because dark noises are produced by thermally-excited carriers, the dark noise rate varies with the temperature. The temperature dependence of dark noise rate is expressed as

$$\text{Dark noise rate} \propto T^{3/2} \exp\left(-\frac{E_g}{2k_B T}\right), \quad (2.5)$$

where  $T$ ,  $k_B$  and  $E_g$  are the absolute temperature, Boltzman's constant, and band gap energy of silicon, respectively.

## 2.2.4 Optical crosstalk

When light enters one MPPC pixel, a pulse of 2 p.e. or higher is sometimes observed. This is because secondary photons are generated in the avalanche multiplication process of the MPPC pixel and those photons are detected by other pixels. This phenomenon is called optical crosstalk. Since the overestimation of a signal is caused by the phenomenon, it affects pulse linearity and dynamic range.

Because the optical crosstalk is also caused by a dark noise, the crosstalk probability can be obtained by measuring dark noise. The crosstalk probability is defined as a ratio of the dark noise rate measured with a 1.5 p.e. threshold to that measured with 0.5 p.e. threshold. The crosstalk probability increases as the overvoltage increases. When the applied overvoltage is constant, it has almost no dependence on the temperature.

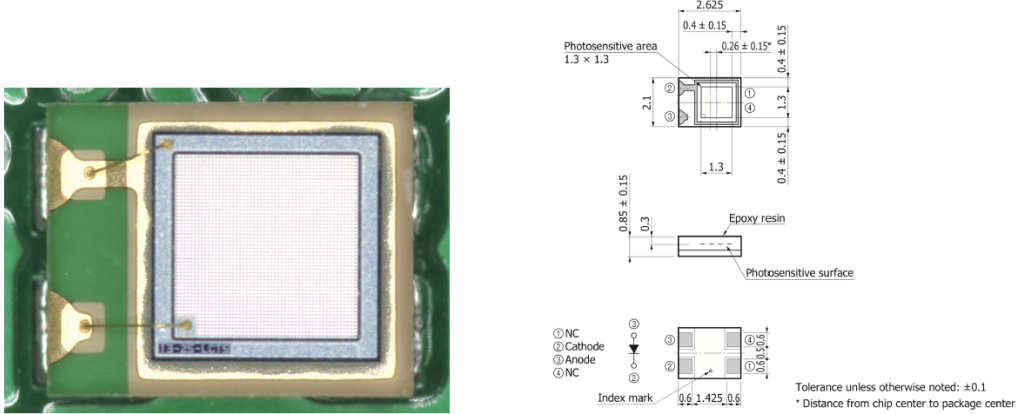


Figure 2.5: Left:picture of the MPPC S13360-1325PE. Right:dimensional specifications of S13360-1325PE [17].

## 2.3 MPPC used for SuperFGD

The MPPCs have been successfully used in all plastic scintillator detectors of the current near detectors of T2K. We also adopt the MPPC for newly developed scintillator detector SuperFGD [16].

### 2.3.1 Specification

The MPPC type used for SuperFGD is S13360-1325PE [17]. Figure 2.5 shows a picture and a drawing of this type of MPPC. The specifications of the S13360-1325PE are summarized in Table 2.2. Its sensitive area is  $1.3 \text{ mm} \times 1.3 \text{ mm}$ , providing enough optical coupling with 1 mm diameter of the WLS fiber. It has 2668 pixels with  $25 \mu\text{m}$  pixel pitch which provide a wide dynamic range. It is needed because the expected light yield in SuperFGD varies from an order of 10 p.e. which is emitted by a minimum ionizing particle to an order of hundred p.e. which is emitted by a stopping proton. The surface mount package was chosen to minimize space and cost. The typical breakdown voltage at  $25 \text{ }^\circ\text{C}$  is 53 V and the recommended operation voltage is 5 V above the breakdown voltage. The peak wavelength of 450 nm matches the emission wavelength of the WLS fiber. Its gain and PDE is enough for measuring a few p.e. level signal. Thanks to the development over the past 10 years, the dark noise rate and the crosstalk probability are much smaller compared to the MPPC used in the current near detectors.

### 2.3.2 MPPC-PCB

Every 64 MPPCs will be mounted on a print circuit board (PCB). Figure 2.6 shows pictures of an MPPC-PCB prototype. On the front side,  $8 \times 8$  MPPCs are placed with a 10.30 mm pitch. On the back side, a 1 k $\Omega$  resistor and a 0.1  $\mu\text{F}$  capacitor are mounted as a low-pass filter for each MPPC, and two temperature sensors (103KT-1608T-1P) are also mounted for monitoring temperature in in-situ operation. The connector (LSHM-140-02.5-L-DV-A-S-K-TR) has 80 pins which are used to supply bias voltage both to MPPCs and temperature sensors and to read out

Item	Specification
Photosensitive area	1.3 mm × 1.3 mm
Pixel pitch	25 $\mu$ m
Number of pixels	2668
Fill factor	47%
Package type	Surface mount
Breakdown voltage	53 $\pm$ 5 V
Peak sensitivity wavelength	450 nm
Photon detection efficiency	25%
Gain	7.0 $\times$ 10 <sup>5</sup>
Dark noise rate	70 kHz
Crosstalk probability	1%

Table 2.2: Specifications of the S13360-1325PE. The characteristics are measured at  $V_{\text{over}} = 5$  V and 25  $^{\circ}$ C

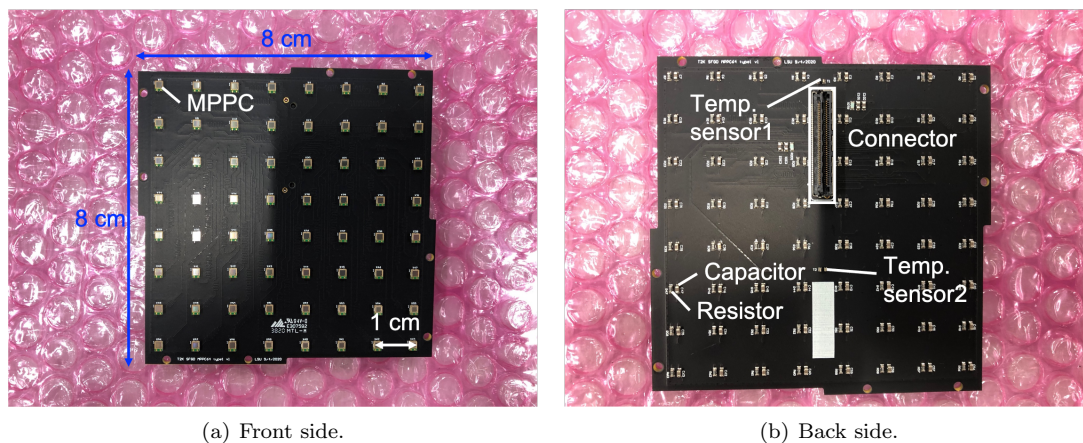


Figure 2.6: Pictures of MPPC-PCB prototype.

the signals of all MPPCs. Two types of PCB with different connector positions are designed to make cable arrangement clear. Each type will be produced in half.

### 2.3.3 Production of MPPC

The number of MPPCs used for SuperFGD is 56,384. All MPPCs have been already produced by Hamamatsu Photonics. Among them, 50,688 MPPCs have been delivered in Japan and the other 10k MPPCs have been delivered in the United States. For the delivery of those MPPCs, 768 MPPCs were packed in a reel as shown in Figure 2.7 and 66 reels have been delivered. Hamamatsu measured the typical operation voltage  $V_{\text{op}} = V_{\text{br}} + 5$  V at 25  $^{\circ}$ C for all MPPCs before shipment and the results are shown in Figure 2.8. Though Hamamatsu gave measurement results for each reel, it is not known which measured value corresponds to which MPPC operation voltage since it is difficult to track all MPPCs in the packing process. According to the results of the measurements by Hamamatsu, the variation of the operation voltages of all MPPCs is within 2.5 V. Also the variation in each reel is within 0.3 V for all reels.

The production of MPPC-PCB will start in April 2021. The total number of MPPC-PCBs

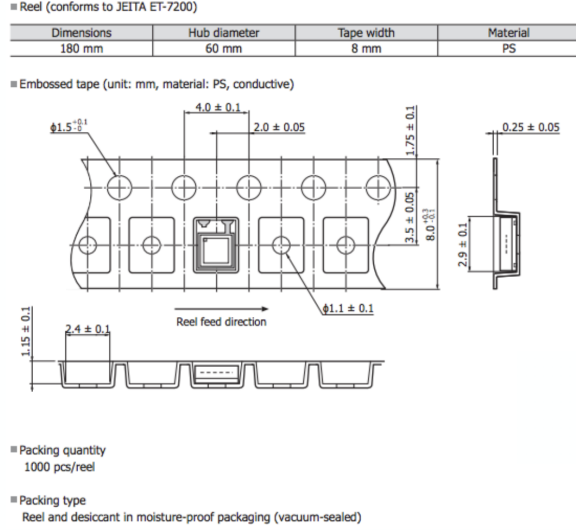


Figure 2.7: Reel package of MPPC.

used in SuperFGD is 881. Among them, 792 PCBs will be produced and be tested in Japan.

## 2.4 Requirements for MPPCs used for SuperFGD

To operate SuperFGD with a good performance, the MPPCs need to meet some requirements. Because the number of MPPCs used in SuperFGD is very large, there may be some MPPCs with strange behaviors. Therefore, the quality assurance of the MPPCs is an important task. The requirements that the basic properties of each MPPC must meet for the operation of SuperFGD is discussed in the following sections.

### 2.4.1 Requirements for operation voltage

To measure scintillation light precisely, it is important that the gains of all MPPCs are uniform. To realize that, a gain calibration will be performed in in-situ operation by adjusting the applied voltage for each MPPC. The range of adjustment is 2.5 V. However, the operation voltage that gives the same gain is different for each MPPC mainly due to the difference in the breakdown voltage. If the variation of operation voltage that gives the same gain in each PCB is greater than 2.5 V, the gain tuning is impossible. Therefore, the variation of the operation voltage which gives the same gain in each PCB should be within the range of 2.5 V.

Based on the measurements of Hamamatsu discussed in Section 2.3.3, the variation of operation voltage in each reel is within 0.3 V for all reels. Therefore, the variation is expected to be within the range of 0.3 V and it is satisfactory for the gain tuning purpose.

### 2.4.2 Requirements for gain and PDE

The uniformity of the gain and the PDE of MPPCs is important especially for the particle identification in SuperFGD. The performance of the particle identification in SuperFGD was studied using the beam test results of the prototype of SuperFGD and showed the capability of

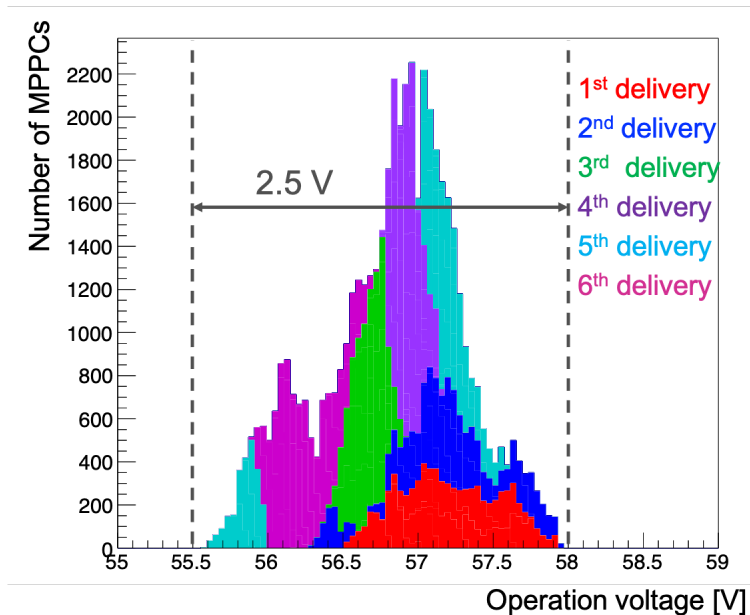


Figure 2.8: Operation voltage measured by Hamamatsu.

distinguishing between muon/pion and proton as described in Section 1.3.3. In the beam test analysis, the uniformity of the readout channel was also studied. Figure 2.9 shows the mean light yield produced by minimum ionizing particles for 384 readout channels. The variation is about  $\pm 25\%$  at maximum. The variation contains not only the non-uniformity of the gain and the PDE of MPPCs but also other factors such as impurities in scintillator cubes, potential failures in the WLS fibers such as cracks, and connection condition between WLS fiber and MPPC. Therefore the variation of the gain and the PDE is considered to be less than  $\pm 25\%$ .

The variation of the gain and the PDE of the same type of the MPPCs used in another near detector of T2K was also studied in a past test [18]. Figure 2.10 shows the distribution of the measured gain and relative PDE of S13360 MPPCs. The variations of gain and relative PDE are about  $\pm 10\%$  at maximum. Based on the results, we require the variation of the gain and the PDE at the typical overvoltage of 5 V is within the  $\pm 10\%$  range. In the operation of SuperFGD, the gain tuning will be performed and the variation can be further reduced. Because the  $\pm 10\%$  variation corresponds to about  $\pm 0.5$  V difference of the operation voltage, it can be adjusted.

### 2.4.3 Requirements for dark noise rate and crosstalk probability

There is a possibility that the MPPC dark noise pulse can be mistakenly counted as a hit of a cube. To estimate such possibility, suppose that all MPPCs have 200 kHz dark noise rate and 3% crosstalk probability which is considered as the maximum case of the MPPCs used for SuperFGD. If we set 1.5 p.e. level threshold, 2 p.e. level noise signal of each MPPC is triggered in 6 kHz rate. The neutrino beam of T2K has bunch structure and each bunch has a time width of  $\sim 50$  ns. Then the probability that one MPPC generates 2 p.e. level dark noise pulse in a bunch  $P_{\text{MPPC}}$  is

$$P_{\text{MPPC}} = 6 \text{ kHz} \times 50 \text{ ns} = 300 \times 10^{-6}. \quad (2.6)$$

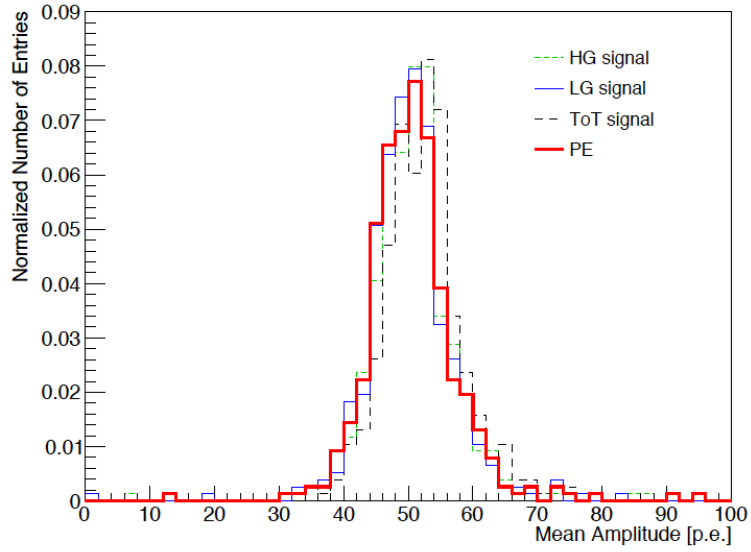


Figure 2.9: Mean light yield produced by minimum ionizing particles for 384 readout channels of the prototype of SuperFGD [13]. Each line shows light yield calculated by a different calibration method. The variation is about  $\pm 25\%$  at maximum in all methods.

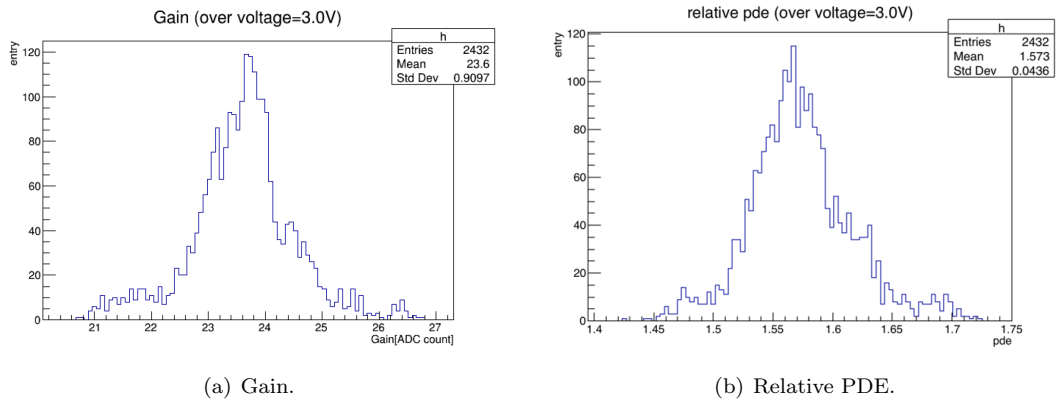


Figure 2.10: The distribution of the gain and the relative PDE of S13360 MPPCs used in another near detector of T2K experiment [18].

Item	Requirements
Gain	Within the range of $\pm 10\%$
Operation voltage	Within the range of $\pm 1.25$ V in each PCB
Relative PDE	Within the range of $\pm 10\%$
Dark noise rate	Less than 200 kHz
Crosstalk probability	Less than 3%

Table 2.3: The requirements for the basic properties of MPPCs used in SuperFGD.

For one cube to be counted as a hit, all MPPCs in three directions from the cube must generate a noise signal. Then, the probability that one cube is counted as a hit  $P_{\text{cube}}$  in a bunch is calculated as

$$P_{\text{cube}} = (P_{\text{MPPC}})^3 = 27 \times 10^{-12}. \quad (2.7)$$

Because SuperFGD uses about two million cubes, the number of the noise hit cube in a bunch  $N_{\text{noise}}$  is calculated as

$$N_{\text{noise}} = 2 \times 10^6 \times P_{\text{cube}} = 54 \times 10^{-6}. \quad (2.8)$$

The number is negligibly small. If the dark noise rate and the crosstalk probability of an MPPC are less than 200kHz and 3%, respectively, there is no problem. For a quality assurance purpose, we require the dark noise rate and the crosstalk probability at the typical overvoltage of 5 V is less than 200 kHz and 3%, respectively.

#### 2.4.4 Summary

The requirements for the basic properties of MPPCs are summarized in Table 2.3.

## Chapter 3

# Development of MPPC performance test system

More than 50,000 MPPCs will be used for SuperFGD and the qualities of those MPPCs must be understood for assuring the performance of SuperFGD. To measure the performance of a large number of MPPCs in a reasonable time frame, we have been developing a test system that measures 512 MPPCs (8 MPPC-PCBs) simultaneously. The gain, relative PDE, dark noise rate, and optical crosstalk probability will be automatically measured with various bias voltages. In this chapter, the purpose, requirements, design, and measurement methods of the test system are described.

### 3.1 Purpose of the performance test

To maximize the performance of SuperFGD, it is important that all MPPCs work properly. We plan to perform the performance test of all MPPCs before the installation of the MPPCs to SuperFGD. Similar performance tests were performed for the MPPCs used in current near detectors of T2K [19, 20, 21, 22]. By the results of the measurements, we will check if each MPPC is not broken and satisfies our requirements. In addition, the measurement result will be used as a reference after the MPPC-PCBs are installed into the detector. Those data are important to understand the performance of SuperFGD.

### 3.2 Measurement items and requirements for the test system

To confirm the performance of each MPPC, we measure six basic properties of MPPCs:

- Gain
- Operation voltage
- Breakdown voltage
- Relative PDE
- Dark noise rate

Item	Requirement for uncertainty
Gain	< 3% (ratio)
Operation voltage	< 0.1 V
Relative PDE	< 3% (ratio)
Dark noise rate	< 5 kHz
Crosstalk probability	< 0.1%

Table 3.1: The requirements for measurement uncertainties of the test system.

- Crosstalk probability

The operation voltage is defined as the applied voltage which gives the gain of  $5.0 \times 10^5$ . The relative PDE is defined as a ratio of the PDE of an MPPC to the PDE of a reference MPPC which is described in Section 3.3.4.

The requirements for those measurement items are discussed in Section 2.4. To confirm each MPPC satisfies our requirements, the measurement uncertainties of the test system should be less than a certain level.

For the operation voltage, although the requirement from electronics is that the variation is within the range of 2.5 V for each PCB, the variation is expected to be less than 0.3 V. To confirm that the variation is sufficiently small, we require that the measurement uncertainty of the operation voltage is less than 0.1 V. Although we also measure the breakdown voltage, the uncertainty of the breakdown voltage measurement is larger than that of the operation voltage measurement due to the extrapolation process in the analysis of the breakdown voltage which will be described in 3.5.3. For this reason, we use the operation voltage to evaluate the variation of the voltage behavior of MPPC.

The requirement for the gain and the relative PDE is that the variation is within the range of  $\pm 10\%$ . To confirm that the variation is within the range, we require that the measurement uncertainties of the gain and relative PDE are less than 3%.

The requirement for the dark noise rate and the crosstalk probability is that the measured value is less than 200 kHz and 3%, respectively. To check each MPPC satisfies the requirements, we require that the measurement uncertainties of the dark noise rate and crosstalk probability are less than 5 kHz and 0.1%, respectively.

The requirements for measurement uncertainties of the test system are summarized in Table 3.1.

### 3.3 Design of the test system

In this section, the design of the test system is described.

#### 3.3.1 Overview

Figure 3.1 shows a schematic view of the test system. The system is designed to measure 8 MPPC-PCBs simultaneously. A light source and a reference MPPC to monitor light intensity are used for each MPPC-PCB and they are placed in a measurement box. All the boxes are placed in two thermostatic chambers. The signals from the MPPCs are readout by NIM EASIROC modules [23]. A function generator is used to send triggers both to the light sources and the EASIROC modules. All the measurements are controlled by a data acquisition (DAQ) PC which communicates with the EASIROCs and the function generator.

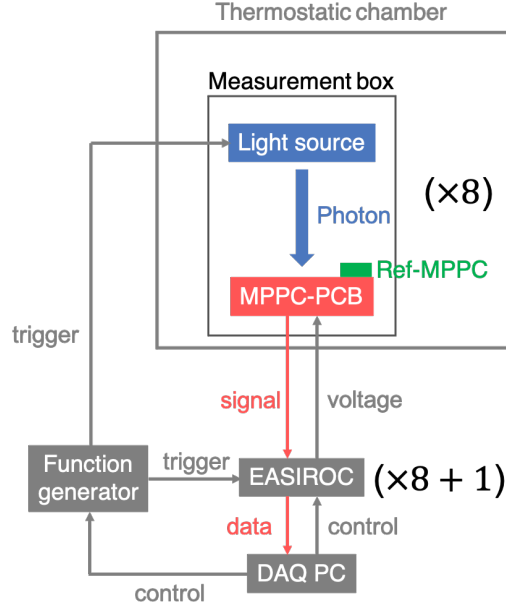


Figure 3.1: Schematic view of the MPPC test system.

### 3.3.2 NIM EASIROC module

In the test system, nine NIM EASIROC modules are used. Among them, eight modules are used for the measurement of eight MPPC-PCBs and an additional module is used for the measurement of reference MPPCs.

The NIM EASIROC module is a general purpose MPPC readout module, developed by Open-It project. Figure 3.2 shows the front side of the module. A NIM EASIROC module controls up to 64 MPPCs by two EASIROC chips [24]. It provides bias voltage for the MPPCs from 0 to 90 V. The bias voltage is monitored by a monitor ADC. Analog signals from the EASIROC chips are converted by four ADCs. An FPGA controls the configuration of the EASIROC chip and data acquisition. Data transfer between the FPGA and DAQ PC is done through Ethernet.

An EASIROC chip controls 32 MPPCs. Figure 3.3 shows block scheme of one channel in an EASIROC chip. The bias voltage applied to each MPPC is individually adjustable within the range of 4.5 V by using a 9-bit input DAC. An EASIROC chip has two amplifiers with high and low gain. A signal after the high gain preamp is shaped by a fast shaper. A discriminator after the fast shaper determines if the pulse height exceeds a given threshold common for all channels. The discriminated signals of 32 channels are sent from the chip to the FPGA in parallel and are counted by a scaler module which is implemented in the FPGA. The signals from the preamps with high and low gain are shaped by slow shapers. Hold circuits after the slow shapers receive a HOLD signal to memorize the voltage of the slow shaper signals at that time. The memorized analog values of high and low gain for all channels are converted by the four ADCs. The bias voltage, the voltage of input DAC, the threshold voltage of discriminator, and the timing of HOLD signal are controllable from DAQ PC.

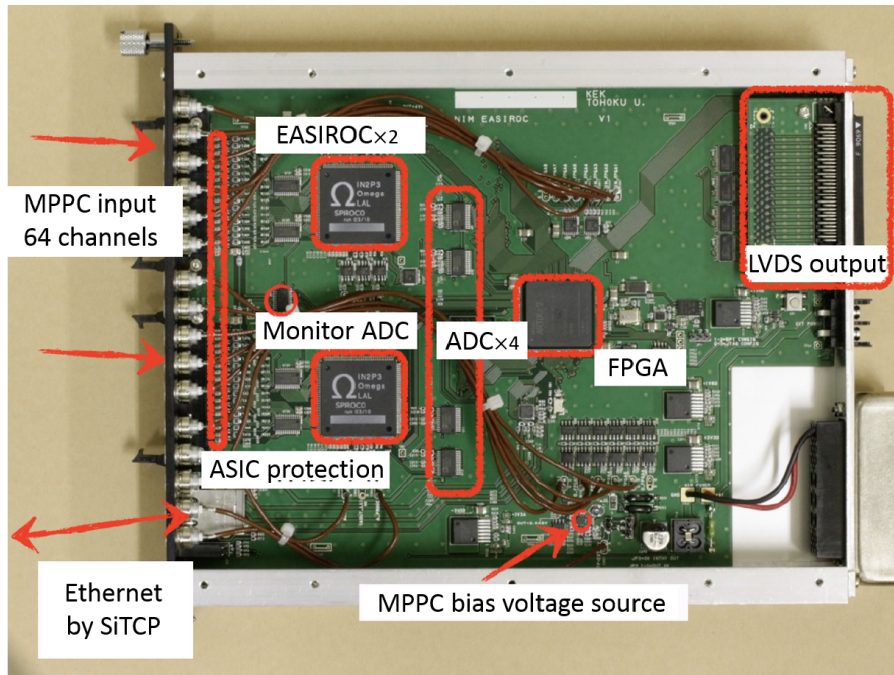


Figure 3.2: The front side of the NIM EASIROC board.

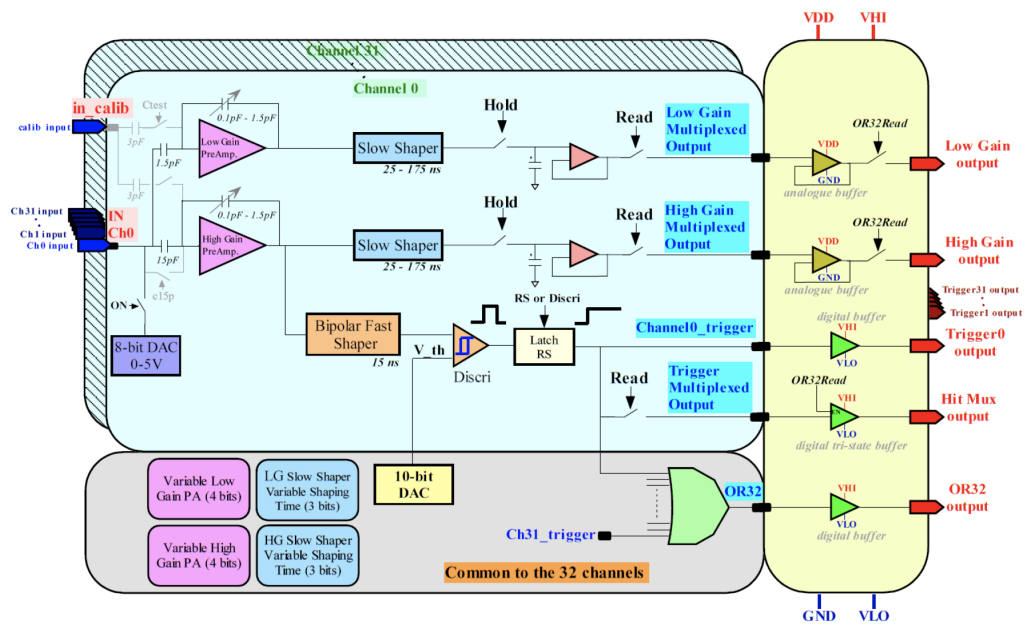


Figure 3.3: The block diagram of an EASIROC chip [24].

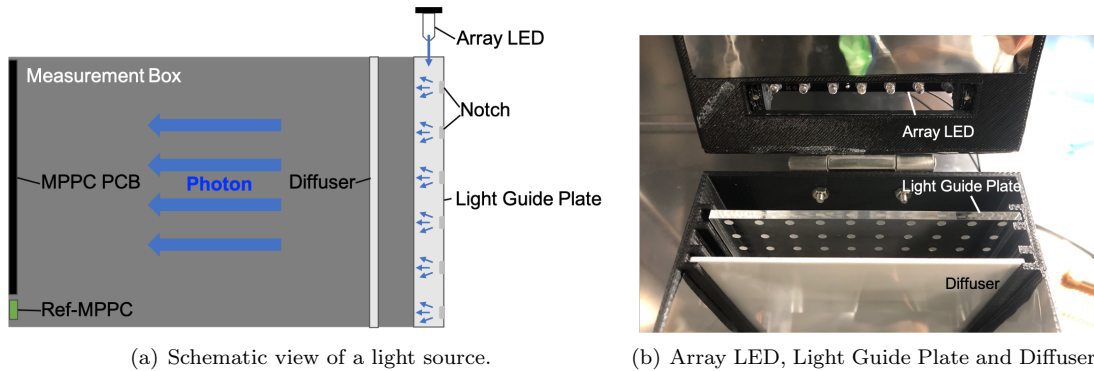


Figure 3.4: Light source used in the test system.

### 3.3.3 Light source

A light source is used to measure the gain and relative PDE. The combination of an LED array, a light guide plate, and a white diffuser is used as a light source. Figure 3.4 shows the schematic view and a picture of the light source.

The LED used in the test system is NSPB300B, Nichia [25]. The peak wavelength of the LED is close to the sensitivity peak of our MPPC and the emission peak of the WLS fiber as shown in Figure 3.5. The LED array consists of seven LEDs which are lined up at 1 cm intervals. The light guide plate is a 10 cm  $\times$  10 cm acrylic plate with notches that scatter light. The notches are arranged in two dimensions at 1 cm intervals. The white diffuser is a 10 cm  $\times$  10 cm glass that diffuses light with wavelengths of 400-700 nm by the Tyndal scattering.

The LED array is fixed to the lid of the measurement box and injects light into the light guide plate. The injected light is scattered by some notches of the light guide plate and propagates towards the MPPC-PCB. The white diffuser is used to improve the light uniformity. The uniformity and stability of the light source will be described in Section 4.1.

### 3.3.4 Reference MPPC

A reference MPPC is used to monitor light intensity and measure relative PDE. The type of the MPPC used for the reference is S13081-050CS and some features are summarized in Table 3.2. The reference MPPC is placed just below the MPPC-PCB as shown in Figure 3.6. One reference MPPC is used for each MPPC-PCB. The signals from the eight reference MPPCs are readout by a NIM EASIROC module via eight coaxial cables. The bias voltage applied to the reference MPPC is fixed at 52.5 V in the performance test.

### 3.3.5 Measurement box

To assure the measurement stability, it is important to maintain the relative position of each element. A measurement box has been developed to fix the MPPC-PCB, the reference MPPC, and the light source. Figure 3.7 shows the measurement box with the lid opened and closed. Though a measurement is performed with the lid closed, we open the lid when replacing the MPPC-PCB. The inside of the box is covered with a mirror sheet to improve light uniformity.

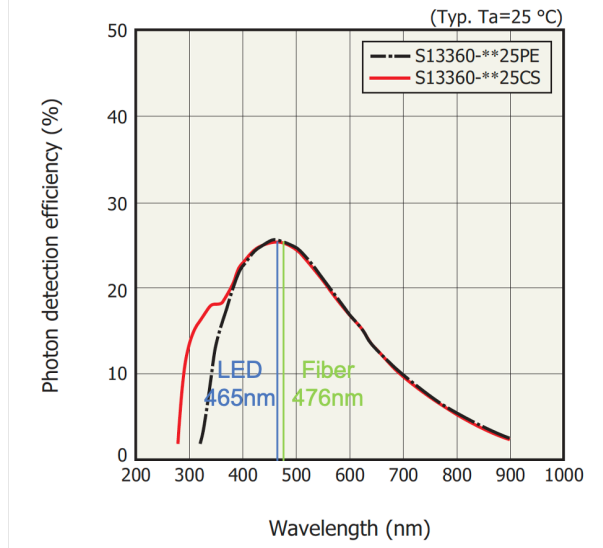


Figure 3.5: Wavelength dependence of PDE of MPPC S13360-1325PE (black line). The blue line shows LED’s peak wavelength. The green line shows the peak emission wavelength of WLS fiber.

Item	Specification
Package type	Ceramic type
Sensitive area size	$1.3 \times 1.3 \text{ mm}^2$
Pixel size	$50 \times 50 \text{ }\mu\text{m}^2$
Number of pixels	667
Operation voltage	54.5 V
Gain	$1.5 \times 10^6$
Peak sensitivity wavelength	450 nm
Photo detection efficiency	35 %
Dark noise rate	90 kHz
Crosstalk probability	1 %

Table 3.2: Specification of the S13081-050CS MPPC used as the reference MPPCs.

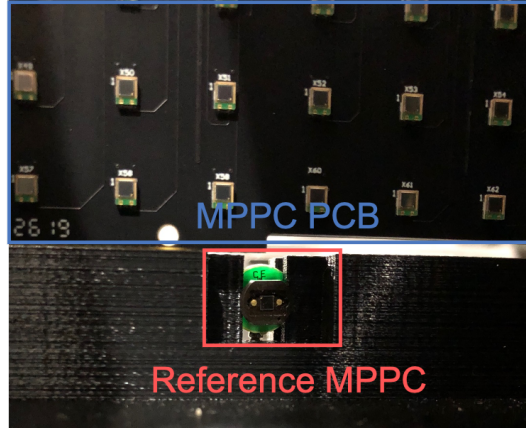
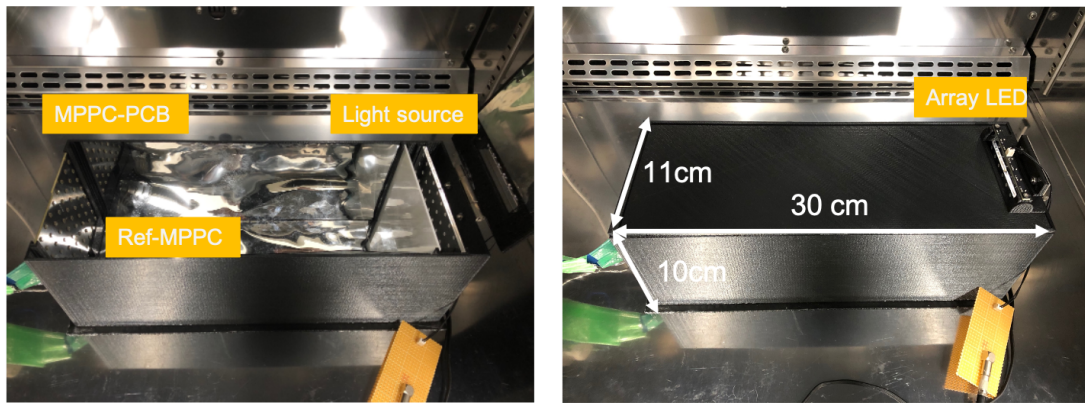


Figure 3.6: The reference MPPC.



(a) Measurement box with lid opened.

(b) Measurement box with lid closed.

Figure 3.7: The measurement box.

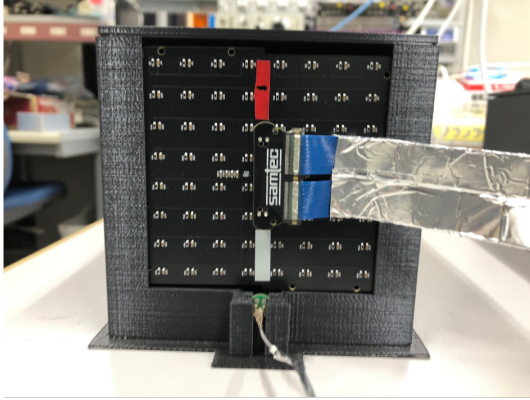


Figure 3.8: The readout cable.

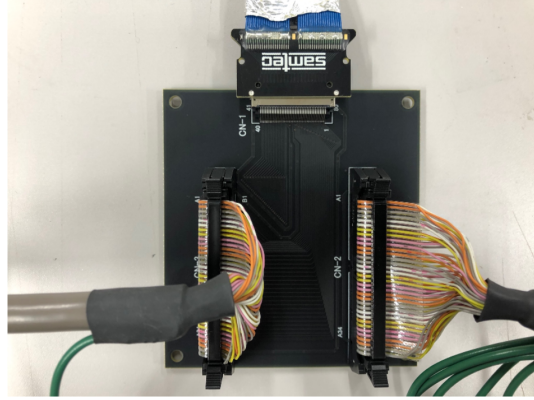


Figure 3.9: The interface board.

### 3.3.6 Readout cable and interface board

Signals from an MPPC-PCB are readout via a flat cable as shown in Figure 3.8. The cable is wrapped with an aluminum tape to suppress the electromagnetic noise. The 64 lines in the flat cable are then divided into 32 lines each on an intermediate board as shown in Figure 3.9. Two flat cables are used to connect the intermediate board and a NIM EASIROC module.

### 3.3.7 Thermostatic chamber

To control the temperature in measurements is important because the properties of MPPC depend on temperature. Two thermostatic chambers are used in the test system. Figure 3.10 shows a picture of the thermostatic chambers, chamber1 (FMU-204I, Fukushima) and chamber2 (INE800, Yamato). According to the size of each chamber, three PCBs and five PCBs are measured in chamber 1 and chamber 2, respectively. The performance test of all MPPCs will be measured at 20 °C which is the typical temperature in the current near detectors.

## 3.4 Measurement method

The performance test system described in the previous section is able to measure the gain, operation voltage, breakdown voltage, relative PDE, dark noise rate, and crosstalk probability. In this section, the measurement methods of those items are presented. Firstly, some parameter tuning of EASIROCs performed before the measurement is described. The DAQ mode used in the performance tests and the measurement flow are explained in the following sections. The analysis method for each measurement item is described in the next section.

### 3.4.1 Configuration of EASIROC

Some parameters of the NIM EASIROCs have been tuned before the performance test. Those parameters will be fixed during all the measurements.



(a) Chamber1.



(b) Chamber2.

Figure 3.10: The thermostatic chambers.

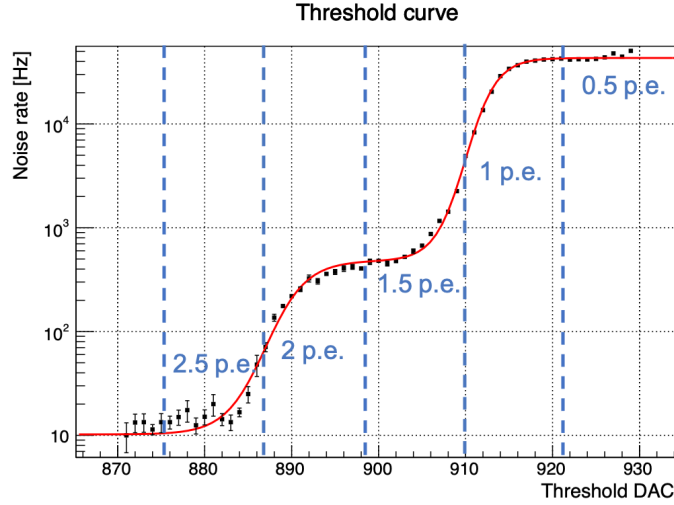


Figure 3.11: Threshold curve

### Threshold DAC

In a NIM-EASIROC module, the MPPC signals which exceed a given threshold are counted by the FPGA scaler. For the measurement of dark noise rate, the signals that exceed 0.5 p.e. threshold level are counted. Therefore, the threshold level must be adjusted to 0.5 p.e. level.

To find the 0.5 p.e. level threshold, we measured the dark noise rate of the 64 channel MPPCs of an MPPC-PCB at 55.5 V as a function of threshold DAC. Figure 3.11 shows an example of the measurement results of an MPPC. The plot is also called a threshold curve or scurve. Since threshold voltage increases as the threshold DAC decreases, the dark noise rate decreases when the threshold DAC is lowered. The data are fitted by a sum of two sigmoid functions and constant. From the fitting parameters, we determine the threshold DAC value of certain p.e. level.

The 0.5 p.e. level threshold DAC is measured for the 64 channels of an EASIROC module. Figure 3.12 shows a distribution of the 0.5 p.e. level threshold DAC for each EASIROC chip of an EASIROC module. The difference between CHIPS is clearly seen. Because the threshold level is common for 32 channels of an EASIROC chip, we decide 0.5 p.e. threshold level for each chip. The 0.5 p.e. level threshold DAC for each chip is defined as the mean value of the 0.5 p.e. level threshold DAC of 32 channels of the chip. The decided 0.5 p.e. level threshold DAC values for 16 chips used for dark noise rate measurement of MPPC-PCBs are summarized in Table 3.3.

The 0.5 p.e. level threshold is decided by the measurements in which the applied bias voltage is 55.5 V. In the performance test, the dark noise rate will be measured at the bias voltages from 55.5 V to 57.4 V. As the applied bias voltage increases, the gain of an MPPC increases. If the threshold is set to the 0.5 p.e. level measured at 55.5 V, 1p.e. level dark noise at higher voltages is always counted. Therefore, the threshold level decided above is fixed for the measurements at all bias voltages.

In the measurements described above, an MPPC-PCB is used to decide the threshold level. However, when measuring another MPPC-PCB with a larger breakdown voltage, the gain is smaller at the same bias voltage. It may cause underestimation of the dark noise rate if we use the same threshold level. To avoid such bias, it is needed to adjust the threshold level for each PCB. We are planning a method to adjust the threshold level according to the gain measurement results of each PCB.

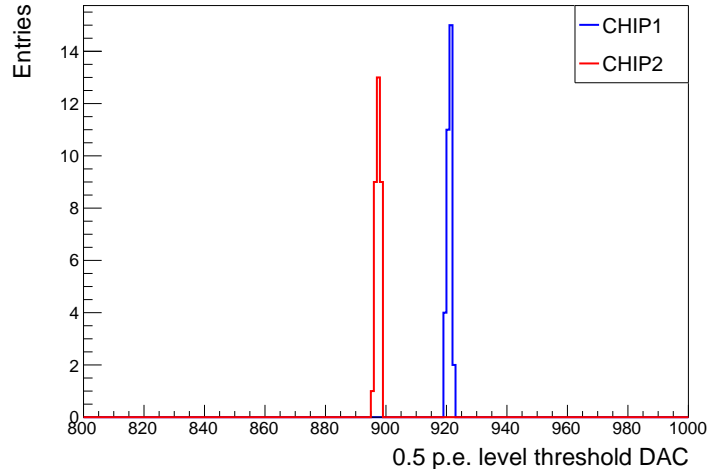


Figure 3.12: The histogram of measured 0.5 p.e. level threshold DAC for each EASIROC chip of an EASIROC module.

Module Number	DAC (CHIP1)	DAC (CHIP2)
1	888	894
2	917	880
3	921	897
4	902	839
5	878	870
6	913	858
7	948	861
8	908	894

Table 3.3: The 0.5 p.e. level threshold DAC for 16 EASIROC chips. The values are decided by the measurements of an MPPC-PCB.

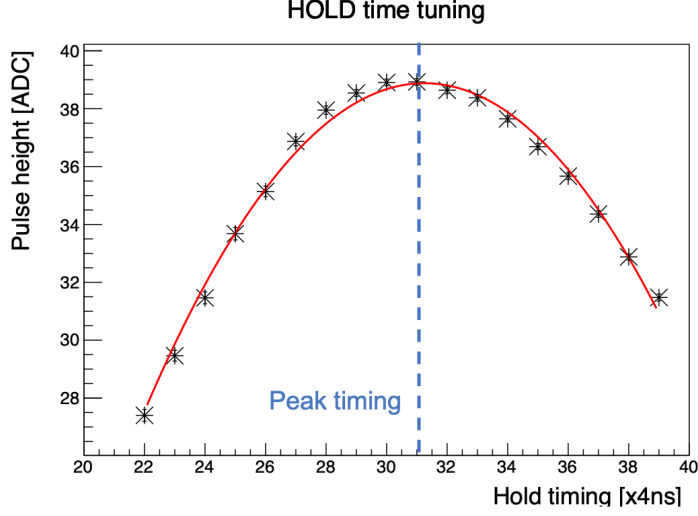


Figure 3.13: Hold time scan. The plot is fitted by a quadratic function (red line).

### HOLD timing

An EASIROC measures the pulse-height of an MPPC by memorizing the voltage of a slow shaper signal at the timing when a HOLD signal is received. If the HOLD signal is earlier or later than the peak timing of the MPPC signal, the pulse height is underestimated. Therefore, HOLD timing must be adjusted to the peak timing of the MPPC signal.

To tune HOLD timing, we measured the pulse-height of MPPC with changing HOLD timing. Figure 3.13 shows an example of the results of the HOLD time scan. By fitting the data with a quadratic function, we determine the hold timing which maximizes the measured signal height. Figure 3.14 shows the histogram of the measured peak timings for all 64 channels. Since HOLD timing is common for all 64 channels of an EASIROC module, we define the HOLD timing of the EASIROC module as the mean value of the distribution. We measure the peak HOLD timing for nine EASIROC modules and there is no big difference in HOLD timing among the modules. Therefore, we set the HOLD timing to 31 for all EASIROC modules.

### Charge-ADC calibration

The analog pulse height information is converted to the digital value by ADC. To reconvert the ADC value to injected charge information, we performed a calibration using a test pulse. An EASIROC chip has calibration inputs for all 32 channel as shown in Figure 3.15. We can inject three different values of test charge to the calibration input from FPGA. Figure 3.16 shows the relation between ADC and injected charge to the calibration input. The plot is fitted by a linear function and the conversion factor from ADC value to injected charge,  $F_{\text{calib}}$ , is defined as the slope of the function. Because the amplification rate of the high gain preamp for test charge is 30 and that for MPPC is 150, the conversion factor for MPPC  $F_{\text{MPPC}}$  must be scaled as

$$F_{\text{MPPC}} = \frac{30}{150} F_{\text{calib}} = \frac{1}{5} F_{\text{calib}}. \quad (3.1)$$

The factor  $F_{\text{MPPC}}$  is used to convert measured MPPC pulse-height in the unit of ADC to charge information.

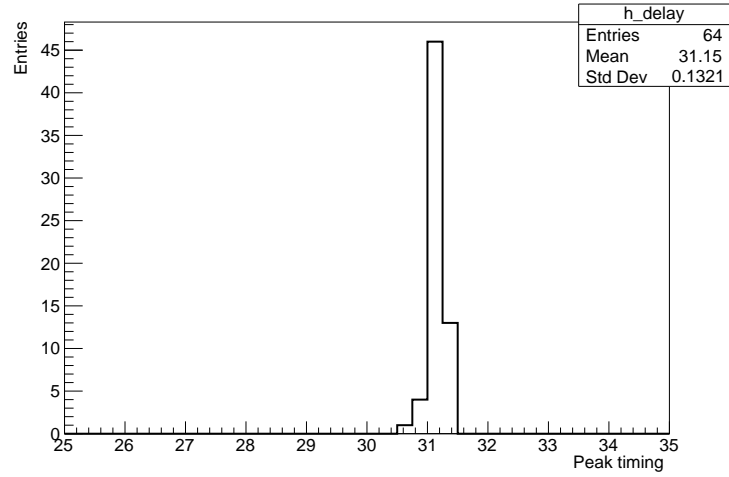


Figure 3.14: The histogram of the measured peak timings for all 64 channels of an EASIROC module.

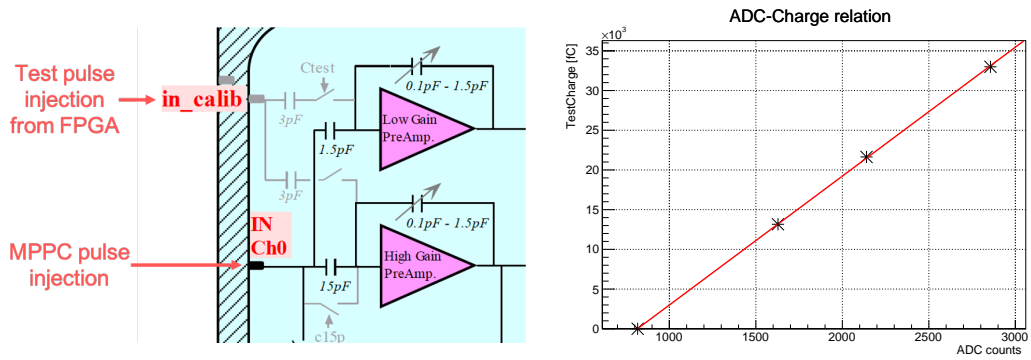


Figure 3.15: The circuit of calibration pulse injection.

Figure 3.16: Relation between ADC and injected charge.

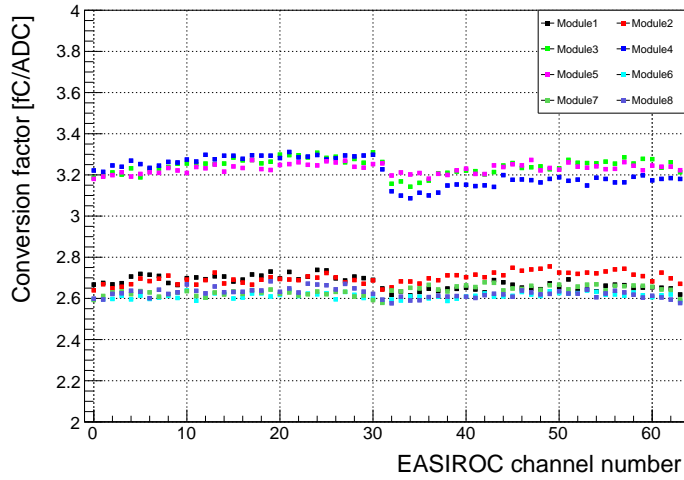


Figure 3.17: The conversion factors for 64 channels of eight EASIROC modules.

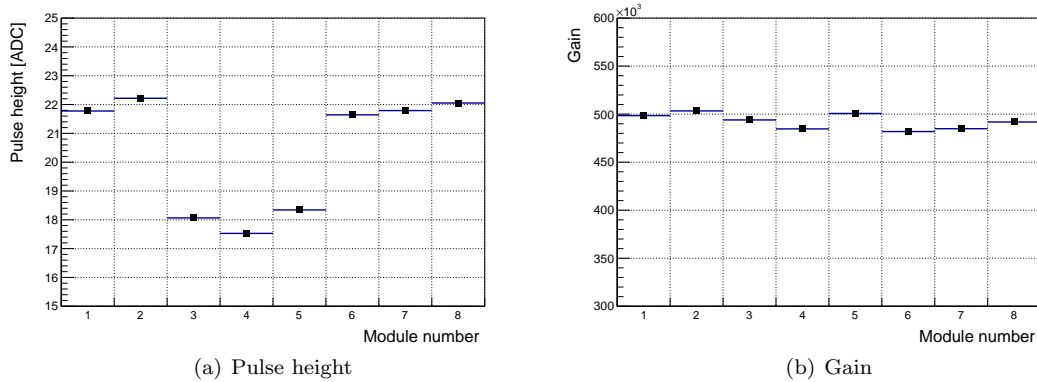


Figure 3.18: The pulse height and the gain of an MPPC measured by eight EASIROC modules.

The conversion factors are measured for all 64 channels of eight EASIROC modules used for the MPPC-PCB measurements. Figure 3.17 shows the measurement results. The factor of module 3, 4, and 5 are larger than those of the other modules. The difference is considered to be due to the difference in versions of the EASIROC chip. The version of the chip used in module 3, 4, and 5 is an old one named SPIROC0 and the version of the chip used in the other modules is a new one named EASIROC1B. The difference is also seen in the pulse height measurement of MPPC. Figure 3.18(a) shows the pulse height of an MPPC measured by eight EASIROC modules. The pulse heights of module 3, 4, and 5 are smaller than those of the other modules. However, it is corrected by multiplying the conversion factor. Figure 3.18(b) shows the gain which is calculated by using the conversion factor. The difference is reduced in the gain and it is found that the correction works properly.

	ADC	Dark noise rate	Scurve
LED	on	off	off
Voltage	20	20	4
Threshold DAC	fixed	fixed	50~90
Time for each point	20 sec	10 sec	1 sec
Total time	~7 min	~5 min	~12 min

Table 3.4: Measurement mode for the performance test.

### 3.4.2 DAQ mode

Three types of DAQ modes are prepared for the performance test.

The first one is ADC measurement mode to measure the gain, operation voltage, breakdown voltage, and relative PDE. In this mode, measurement is performed with LED turned on and the external trigger rate of DAQ is 2 kHz. ADC data is taken at twenty bias voltages from 55.5 V to 57.4 V at 0.1 V intervals. At each voltage, 40,000 events data are taken and it takes 20 seconds. The total time for ADC measurement is about 7 minutes.

The second mode is dark noise rate measurement mode to measure the dark noise rate. In this mode, measurement is performed with LED turned off. Scaler data is taken at twenty bias voltages from 55.5 V to 57.4 V at 0.1 V intervals. At each voltage, data is taken for 10 seconds. The total time for dark noise rate measurement is about 5 minutes.

The last mode is scurve measurement mode to measure the crosstalk probability. In this mode, measurement is performed with LED turned off. Scaler data is taken with changing the threshold level of the discriminator. The number of measured threshold DAC points is 50~90 which varies depending on the applied voltage and used EASIROC chip because of differences of the gain. At each threshold DAC, scaler data is taken for a second. The threshold scan is performed at four bias voltages, 55.5 V, 56.0 V, 56.5 V and 57.0 V. The total time for scurve measurement is about 12 min.

The settings of measurement mode are summarized in Table 3.4.

### 3.4.3 Measurement flow

The procedure of the data taking in the performance test is following

1. Set 8 MPPC-PCBs in the measurement boxes and connect the PCBs with readout cables
2. Wait until the temperature of the PCBs becomes stable
3. Start the main program of DAQ and perform measurements automatically
  - (a) Increase the applied voltage to 55.5 V
  - (b) Make function generator send trigger of LED ON mode
  - (c) Take ADC data from 55.5 V to 57.4 V at 0.1 V intervals
  - (d) Decrease the voltage applied to the MPPCs to 55.5 V
  - (e) Make function generator send trigger of LED OFF mode
  - (f) Take dark noise rate data from 55.5 V to 57.4 V at 0.1 V intervals
  - (g) Decrease the voltage applied to the MPPCs to 55.5 V
  - (h) Take scurve data from 55.5 V to 57.0 V at 0.5 V intervals

- (i) Decrease the voltage applied to the MPPCs to 0 V
- 4. Check data quality after finishing the main program
- 5. Take 8 MPPC-PCBs out of the thermostatic chamber

The procedure will be repeated in the performance test.

It takes about 30 minutes to perform the main measurement. It also takes about 30 minutes to change MPPC-PCBs and wait until the temperature becomes stable. So in total, time for one cycle of measurement is about 1 hour. If we measure 5 cycles per day, we can measure 40 PCBs in a day. The number of PCBs which will be tested in Japan is 792. Therefore, it takes about twenty working days to measure all 50,688 MPPCs.

## 3.5 Analysis method

In this section, the analysis methods for the gain, operation voltage, breakdown voltage, relative PDE, dark noise rate, and crosstalk probability are described. The data used in this section are obtained from measurements of a prototype of MPPC-PCB. They are used to describe the analysis methods.

### 3.5.1 Gain

A typical ADC distribution with LED on is shown in Figure 3.19(a). Peaks corresponding to 0 p.e. (pedestal) events, 1 p.e. events, and so on can be clearly identified. The pedestal peak and 1 p.e. peak are fitted by a sum of two Gaussian functions. The 1 p.e. level pulse-height of the MPPC,  $H$ , is defined as the difference of ADC counts between pedestal peak and 1 p.e. peak:

$$H = (\text{ADC counts of 1p.e. peak}) - (\text{ADC counts of pedestal peak}). \quad (3.2)$$

The output charge of the MPPC,  $Q$ , is calculated by multiplying the conversion factor  $F_{\text{MPPC}}$  as explained in section 3.4.1:

$$Q = F_{\text{MPPC}} \times H. \quad (3.3)$$

Then the gain as a multiplication factor is obtained by dividing  $Q$  by the elementary charge  $e$ :

$$\text{Gain} = \frac{Q}{e}. \quad (3.4)$$

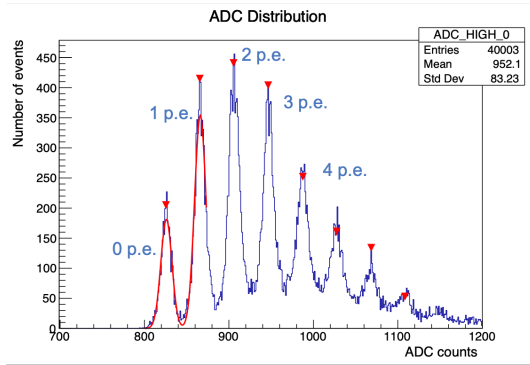
Figure 3.19(b) shows gain as a function of bias voltage. The gain increases linearly as the bias voltage increases.

### 3.5.2 Operation voltage

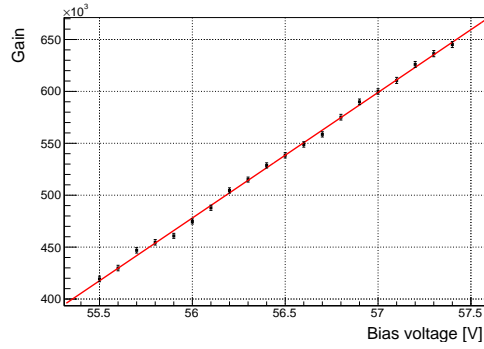
As shown in Figure 3.19(b), the gain-voltage relation is fitted by a linear function. The operation voltage which gives the gain of  $5.0 \times 10^5$  is calculated by the fitted function.

### 3.5.3 Breakdown voltage

The breakdown voltage  $V_{\text{br}}$  is measured by linearly extrapolating the gain-voltage relation to the point where gain becomes zero as shown in Figure 3.20(a). From the breakdown voltage  $V_{\text{br}}$ , we can calculate the overvoltage  $V_{\text{over}} = V_{\text{bias}} - V_{\text{br}}$ . The measured gain as a function of overvoltage is shown in Figure 3.20(b). The error bar of overvoltage is the error bar of the breakdown voltage.

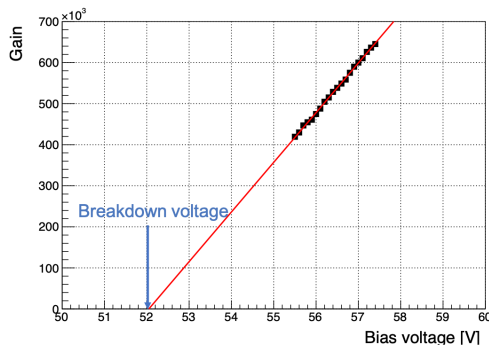


(a) The ADC distribution of an MPPC.

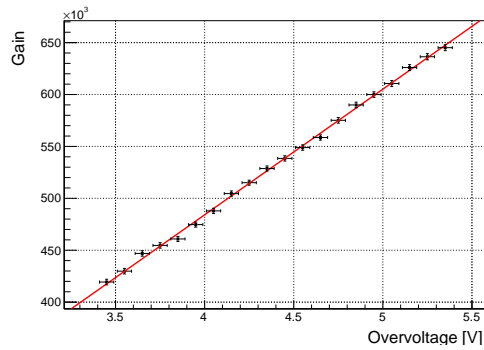


(b) The Gain as a function of bias voltage.

Figure 3.19: The gain measurement.



(a) Determination of  $V_{br}$  from gain-voltage extrapolation.



(b) Gain as a function of overvoltage.

Figure 3.20: The breakdown voltage and overvoltage measurement.

Reference MPPC Number	Relative PDE
1 (standard MPPC)	1.00
2	$0.99 \pm 0.01$
3	$0.98 \pm 0.01$
4	$1.00 \pm 0.01$
5	$1.00 \pm 0.01$
6	$1.00 \pm 0.01$
7	$1.00 \pm 0.01$
8	$0.99 \pm 0.01$

Table 3.5: The relative PDE of the reference MPPCs to a standard MPPC

### 3.5.4 Relative PDE

The relative PDE is calculated as the ratio of the number of photons detected by each MPPCs to the number of photons detected by the reference MPPC:

$$\text{Relative PDE} = \frac{\text{Number of photons detected by each MPPC}}{\text{Number of photons detected by the reference MPPC}}. \quad (3.5)$$

The number of photons detected by MPPC is calculated as follows. Let  $P_n$  be the probability that  $n$  photons are detected by the MPPC. Assuming the number of detected photons follow the Poisson distribution,  $P_n$  is represented as

$$P_n = \frac{\lambda^n}{n!} e^{-\lambda}, \quad (3.6)$$

where  $\lambda$  is the mean value of the number of detected photons. Then,  $\lambda$  can be calculated as

$$P_0 = e^{-\lambda} \Rightarrow \lambda = -\ln(P_0). \quad (3.7)$$

We can calculate  $P_0$  from the ADC distribution as

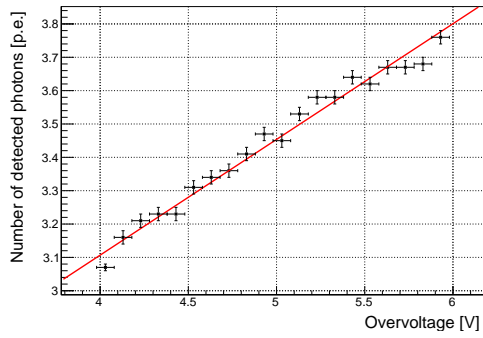
$$P_0 = \frac{\text{Number of pedestal events}}{\text{Number of total events}}. \quad (3.8)$$

Therefore, we can calculate the mean value of the number of photons detected by the MPPC. Figure 3.21(a) shows the number of detected photons as a function of overvoltage.

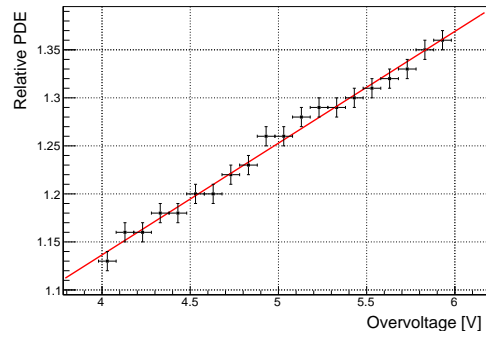
Because eight different MPPCs are used as a reference for each MPPC-PCB, the differences in PDE among the reference MPPCs should be considered. To check the differences, the relative PDE of the reference MPPCs to a standard MPPC is measured beforehand and the results with statistical errors are summarized in Table 3.5. There is no big difference in the PDE of reference MPPCs and the differences are within the range of statistical uncertainty. Therefore, we consider the PDEs of the reference MPPCs are the same. The uncertainty of 1% is evaluated as one of the systematic uncertainty of the relative PDE measurement.

### 3.5.5 Dark noise rate

The dark noise rate is measured by an LED off data. The signals that exceed the 0.5 p.e. level threshold are counted by EASIROC FPGA scaler and the dark noise rate is calculated every 0.1 seconds. Figure 3.22(a) shows the dark noise rate distribution. In the analysis, the dark noise rate is defined as the mean value of the distribution. Figure 3.22(b) shows the dark noise rate as a function of overvoltage. The dark noise rate is linearly increasing as overvoltage increases.

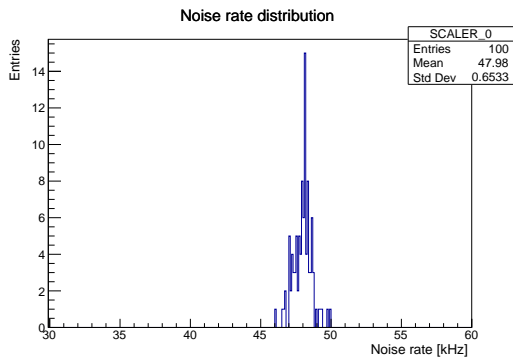


(a) The number of detected photons.

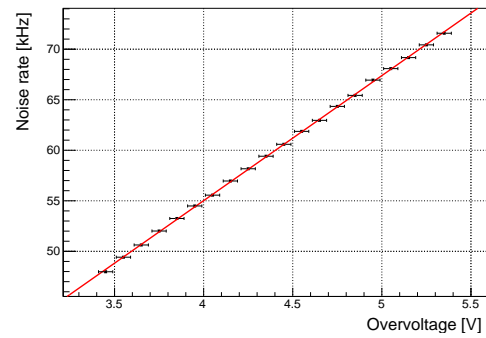


(b) The relative PDE.

Figure 3.21: Overvoltage dependence of the number of detected photons and the relative PDE.



(a) Dark noise rate distribution.



(b) Dark noise rate as a function of overvoltage.

Figure 3.22: The dark noise rate measurement.

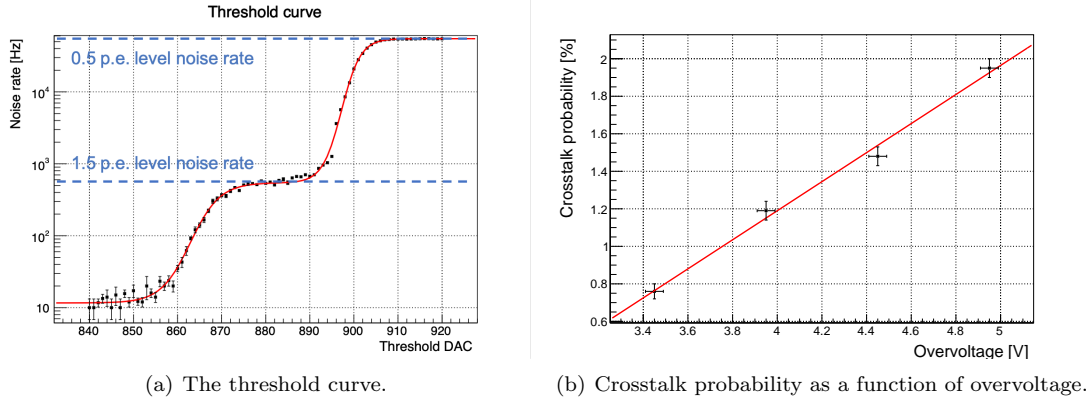


Figure 3.23: The crosstalk probability measurement.

### 3.5.6 Crosstalk probability

The optical crosstalk probability is defined as the ratio of the dark noise rate with 0.5 p.e. and 1.5 p.e. level threshold. Figure 3.23(a) shows dark noise rate as a function of threshold DAC. The data are fitted by a sum of two sigmoid functions and constant. From the fit parameters, we obtain the dark noise rate with 0.5 p.e. and 1.5 p.e. level threshold. Then the crosstalk probability is calculated as

$$\text{Crosstalk probability} = \frac{\text{The darknoise rate over 0.5p.e. threshold}}{\text{The darknoise rate over 1.5p.e. threshold}}. \quad (3.9)$$

Figure 3.23(b) shows the measured crosstalk probability as a function of overvoltage. The crosstalk probability increases as overvoltage increases.

## Chapter 4

# Performance of the test system

In order to confirm each MPPC satisfies our requirements, the test system must meet the requirements discussed in Section 3.2. In this section, the performance evaluations of the test system are presented. In the first section, the evaluations of light uniformity and stability are described. The measurement stability and the module dependence of measurements are evaluated in the following sections. Finally, the systematic uncertainties of the test system are summarized.

### 4.1 Light uniformity and stability

It is important that the light intensity is uniform and stable for the measurement of the relative PDE. The evaluation of light uniformity and stability is presented in this section.

#### 4.1.1 Light uniformity

The uniformity of the light intensity is evaluated by using 64 channel MPPCs on a PCB. The number of detected photons is measured by each MPPC at 55.5 V. The light uniformity is evaluated as a ratio of the standard deviation to the mean value of the 64 channel MPPCs, although it includes not only the spacial non-uniformity but also the variation of PDE of 64 MPPCs. The uniformity is required to be less than 3%.

Firstly, a measurement is performed in a prototype of the measurement box as shown in Figure 4.1. An array of LEDs and a light guide plate (LGP) are used as a light source and the light is diffused by a white diffuser. Figure 4.2 shows the distribution of the light intensity. The uniformity is 7.6% and it does not meet our requirement. Obviously, the light intensity at the center of the PCB is larger than that at the edge of the PCB.

To improve the uniformity, we cover the inside of the measurement box with a mirror sheet to supply more light to the edge of the PCB as shown in Figure 4.3. The result of the light intensity measurement with the mirror sheet is shown in Figure 4.4. The light intensity is relatively larger in the edge of the PCB compared to the measurement without the mirror sheet and the uniformity improves to 2.3%.

The dependence of the light uniformity on the positions of the light source is also checked to decide the positions of the light guide plate and the diffuser. The number of detected photons is measured by the MPPC-PCB with changing the positions of the LGP and the diffuser as shown in Figure 4.5. The position of LGP and the position of the diffuser can be changed in 3 places and 34 places, respectively. Figure 4.6 shows the relation between the light uniformity and the

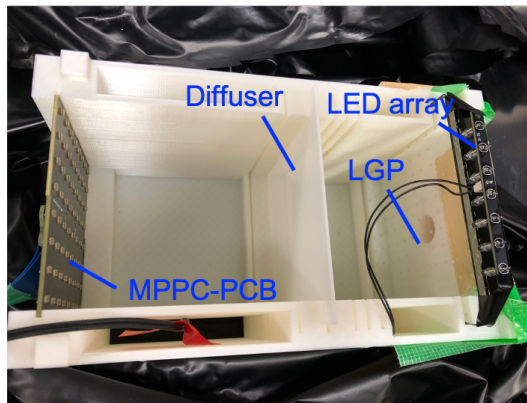
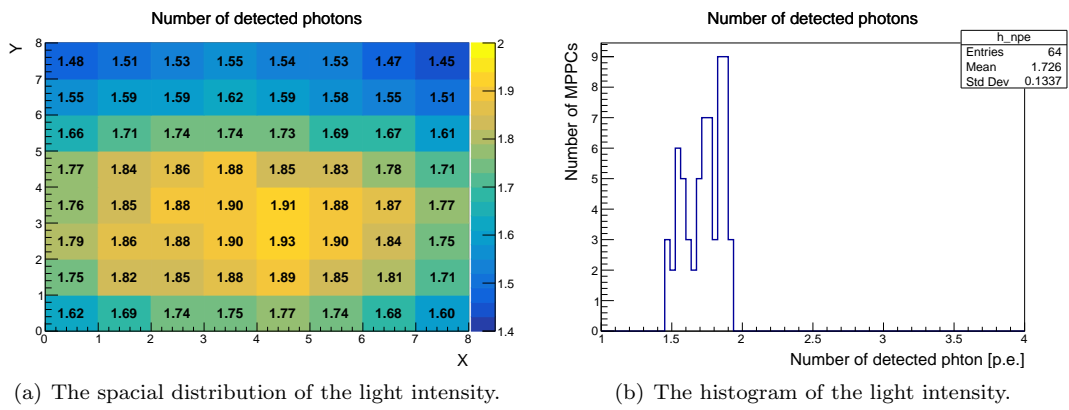


Figure 4.1: A prototype of measurement box.



(a) The spacial distribution of the light intensity.

(b) The histogram of the light intensity.

Figure 4.2: The distribution of the light intensity measured in a prototype of the measurement box

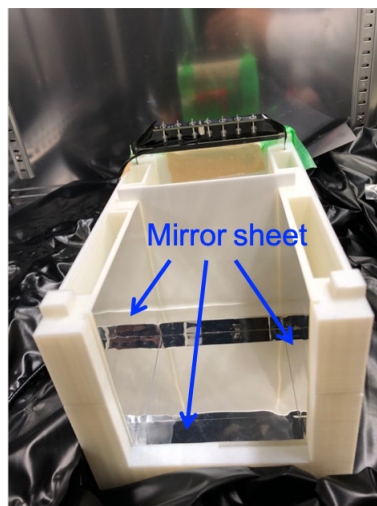


Figure 4.3: The measurement box with mirror sheet.

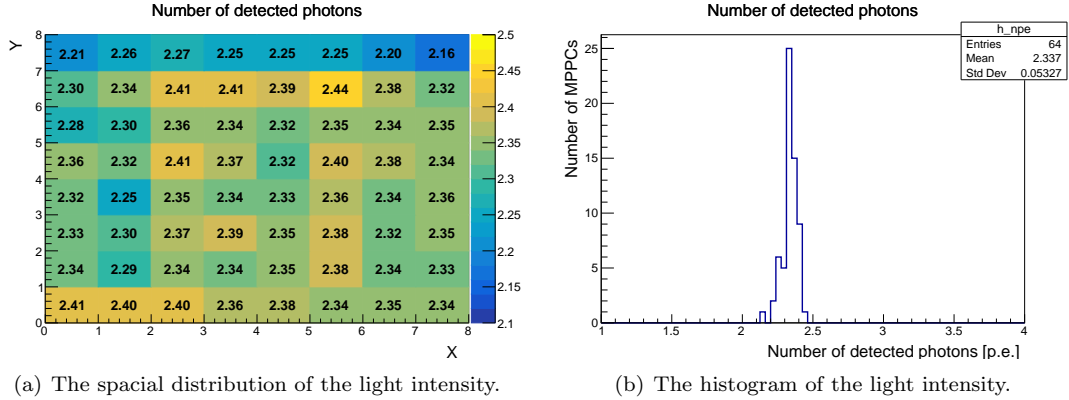


Figure 4.4: The distribution of the light intensity measured with the mirror sheet.

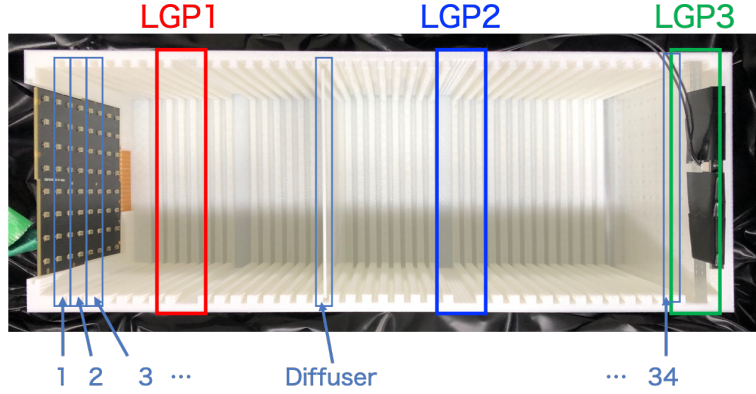


Figure 4.5: The measurement setup for testing dependence of the light uniformity on the positions of the light sources.

positions of the light sources. It is found that the light uniformity is best when the LGP and the diffuser were placed farthest from the MPPC-PCB.

Based on those measurement results, we decided the final design of the measurement box. The produced measurement box is shown in Figure 3.7. The light sources are placed farthest from the PCB and the inside of the box is covered with a mirror sheet. The number of detected photons is measured by the MPPC-PCB in the measurement box. The result is shown in Figure 4.7 and the uniformity is 1.5%. Because the measured value of 1.5% includes both of the spacial variation of the light intensity and the variation of the PDE of 64 MPPCs, it is concluded that the spacial variation of the light intensity is less than 1.5%. The uniformity achieved in the measurement box with the final design is satisfactory for our quality assurance purpose.

#### 4.1.2 Light stability

The stability of the light intensity is also evaluated. The number of detected photons is measured several times by the 64 channel MPPCs on a PCB. In the light stability measurements, the light intensity is evaluated as the mean value of the 64 channel MPPCs to avoid the effect of

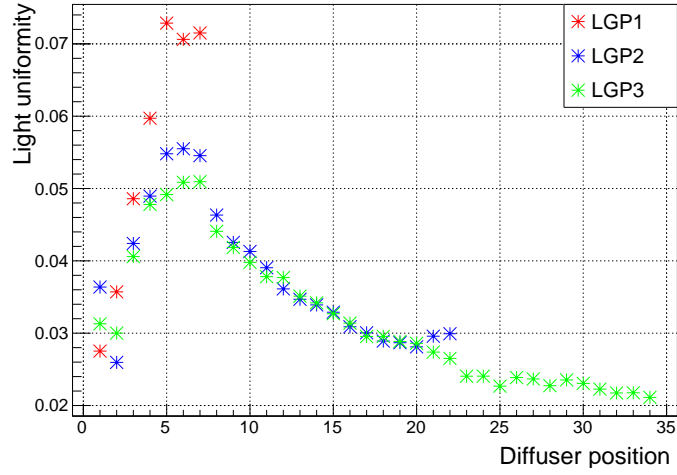
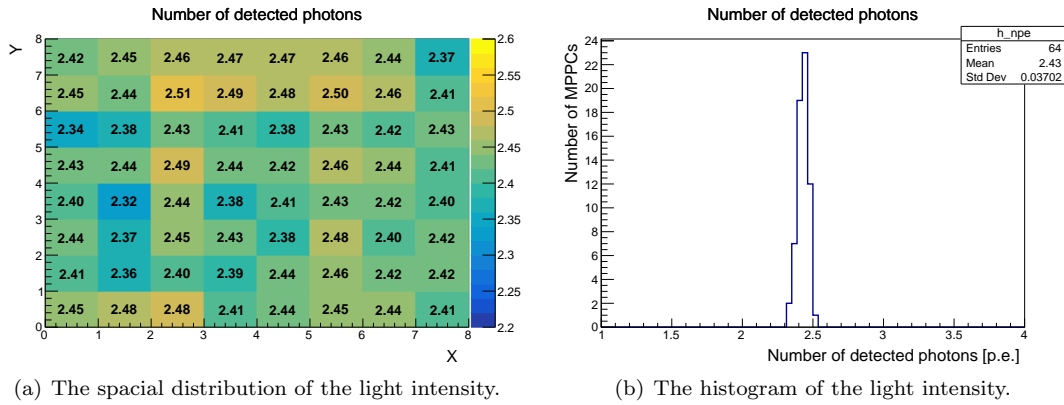


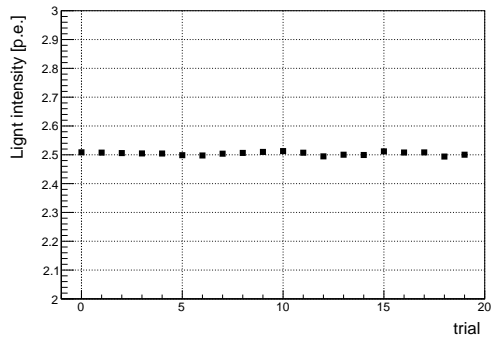
Figure 4.6: The relation between the light uniformity and the position of the diffuser.



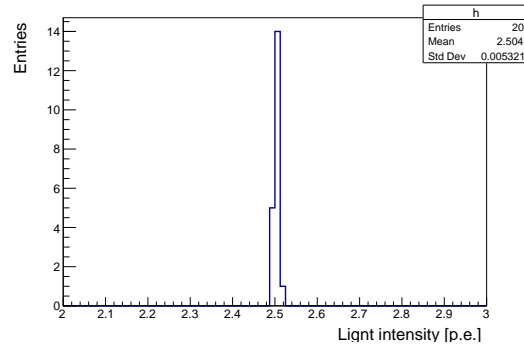
(a) The spacial distribution of the light intensity.

(b) The histogram of the light intensity.

Figure 4.7: The distribution of the light intensity measured in the final design box.

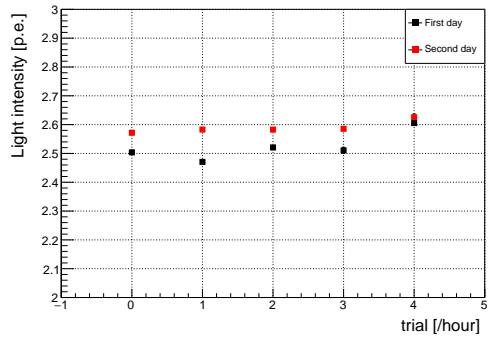


(a) The light intensity in each measurement.

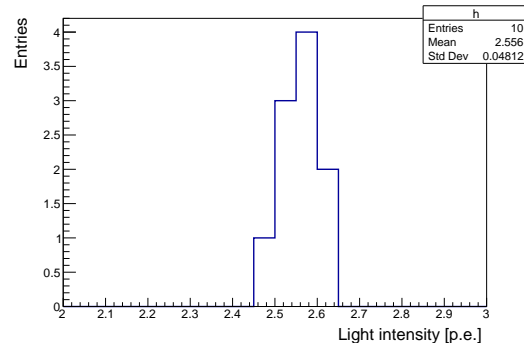


(b) The histogram of the light intensity.

Figure 4.8: The result of the light stability measurement in a short period of time.



(a) The light intensity in each measurement.



(b) The histogram of the light intensity.

Figure 4.9: The result of the light stability measurement in a middle period of time.

fluctuation of each MPPC. The light stability is evaluated as a ratio of the standard deviation to the mean value of the multiple measurements.

Firstly, the light intensity is measured twenty times at twenty seconds intervals to check the stability in a short period. Figure 4.8 shows the measurement results of the light intensity. The variation is 0.2% and it is almost negligible compared to the requirement of 3%.

To check the light stability in a middle period, we measure the light intensity five times at hour intervals in two days. As shown in Figure 4.9, the variation is 1.9% and it is larger than that in the short period. The light intensity on the second day is larger than that on the first day. However, such fluctuations can be corrected by the reference MPPC which is placed just below the MPPC-PCB to monitor the light intensity. Figure 4.10 shows the measurement results of the relative PDE which is defined as a ratio of the light intensity to the number of photons detected by the reference MPPC. The difference between the first day and the second day is not seen in the relative PDE and the variation of the relative PDE is 0.6%. It is found that the correction of the light intensity by the reference MPPC works properly. Therefore, if the light intensity fluctuates in the period of the performance tests, the effect on the measurement of relative PDE is small.

Because the fluctuation of the light intensity is corrected by the reference MPPC, the stability

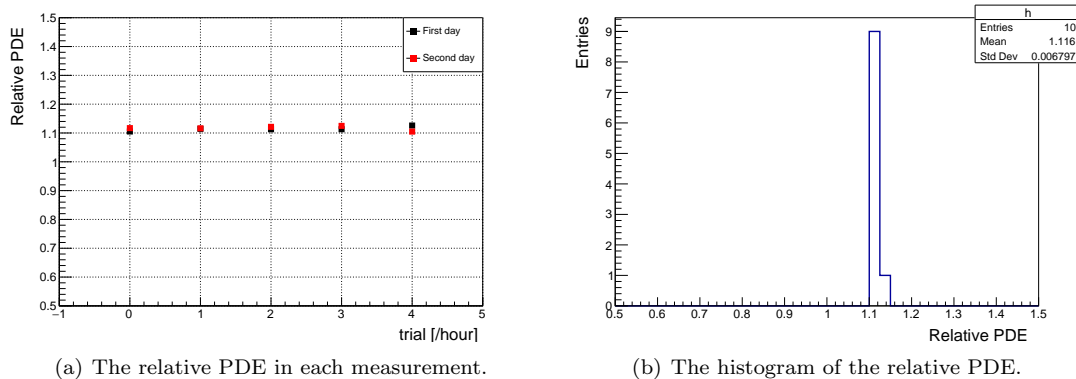


Figure 4.10: The measurement of relative PDE.

of the measurements of the reference MPPC is important. The stability of the reference MPPC will be monitored in the period of the performance test by checking the stability of the gain of the reference MPPC which is not affected by the light intensity. The stability of the gain measurement is typically 1% level as shown in the next section. Therefore, if the gain fluctuates by 3% or more in the period of the performance test, we judge that there is something unstable in the measurements of the reference MPPC and perform an investigation.

## 4.2 Stability of measurement

Measurement results may vary even when measured with the same setup. To evaluate the variation, we measured the gain, breakdown voltage, relative PDE, dark noise rate, and crosstalk probability several times with the same setup.

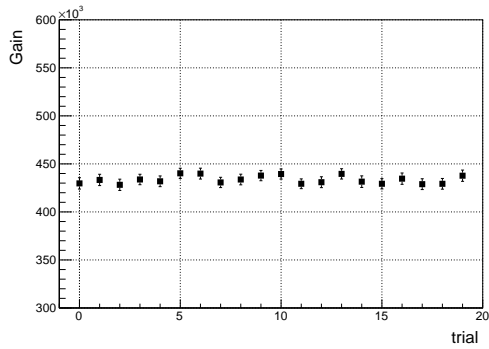
### 4.2.1 Gain

Firstly, the gain is measured at 55.5 V twenty times at twenty seconds intervals. Figure 4.11 shows the measurement results of the gain of an MPPC. The mean value of the twenty measurements is  $4.3 \times 10^5$  and the standard deviation is  $0.04 \times 10^5$ . The ratio of the standard deviation to the mean is 0.9% and it meets the requirement of 3%.

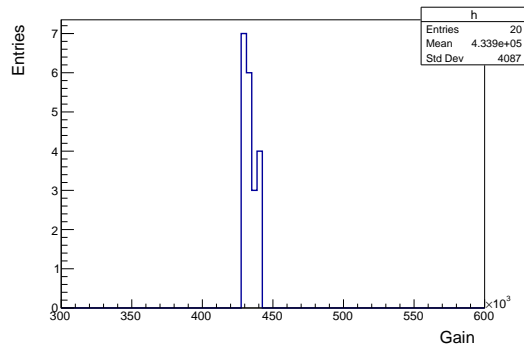
To check the stability in the middle period, we also measure the gain five times at hour intervals in two days. Figure 4.12 shows the measurement results of the gain in each trial. The ratio of the standard deviation to the mean is 1.0%. There is no significant difference in the variation of gain between short period and middle period measurements.

### 4.2.2 Operation voltage

The operation voltage is measured five times at ten minutes intervals. For each measurement, the gain scan at the operation voltages from 55.5 V to 57.4 V as described in the section 3.5.1 is performed. Figure 4.13 shows the measurement results of the operation voltage. The mean value of the five measurements is 56.01 V and the standard deviation is 0.01 V. It satisfies the requirement of 0.1 V.

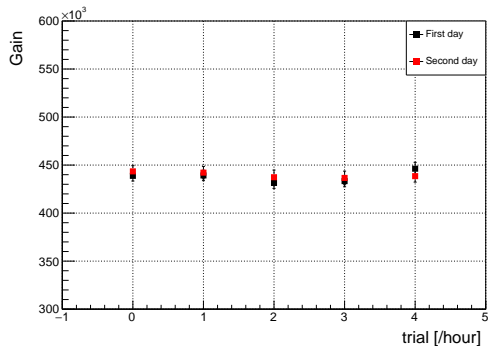


(a) The gain in each measurement.

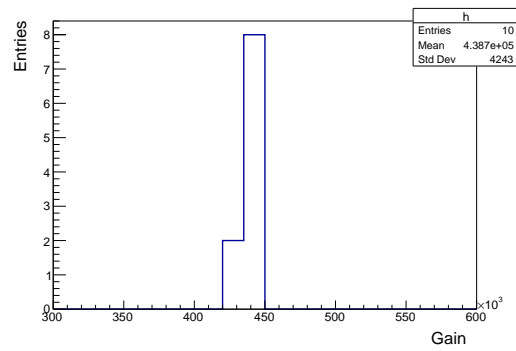


(b) The histogram of the gain.

Figure 4.11: Twenty measurement results of the gain of an MPPC.

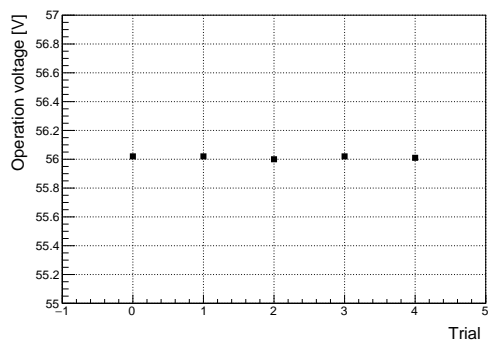


(a) The gain in each measurement.

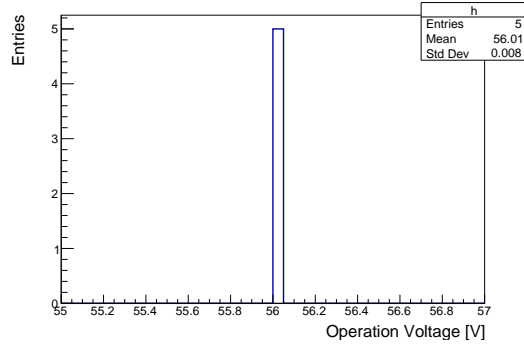


(b) The histogram of the gain.

Figure 4.12: The result of the gain measurement in a middle period of time.

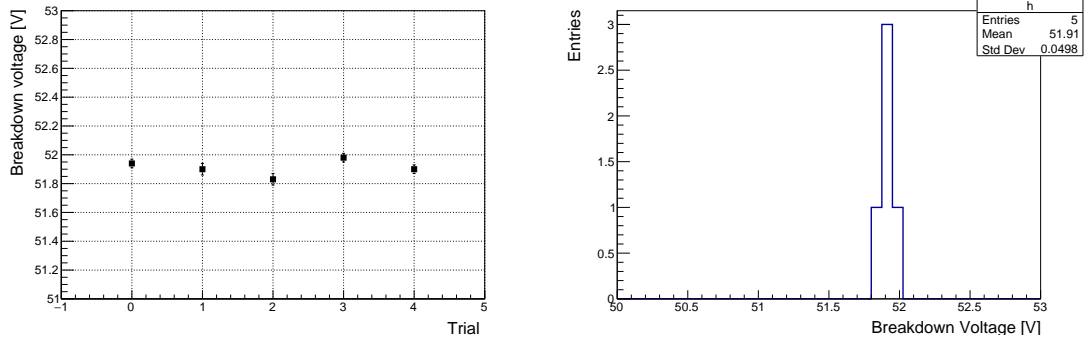


(a) The operation voltage in each measurement.



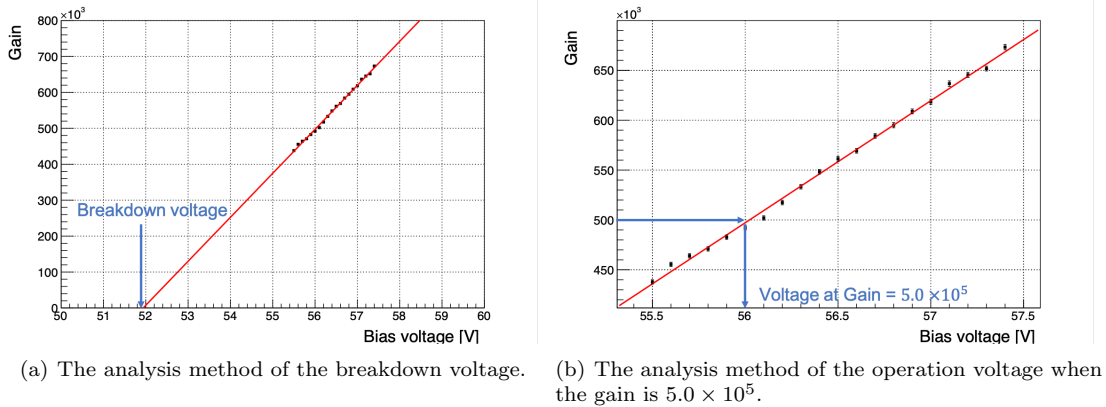
(b) The histogram of the operation voltage.

Figure 4.13: Five measurement results of the operation voltage when the gain is  $5.0 \times 10^5$  of an MPPC.



(a) The breakdown voltage in each measurement. (b) The histogram of the breakdown voltage.

Figure 4.14: Five measurement results of the breakdown voltage of an MPPC.



(a) The analysis method of the breakdown voltage. (b) The analysis method of the operation voltage when the gain is  $5.0 \times 10^5$ .

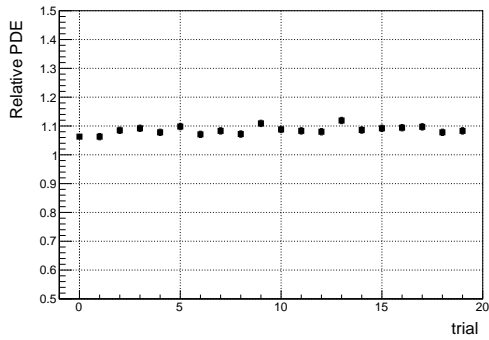
Figure 4.15: The analysis method of the breakdown voltage and the operation voltage when the gain is  $5.0 \times 10^5$ .

### 4.2.3 Breakdown voltage

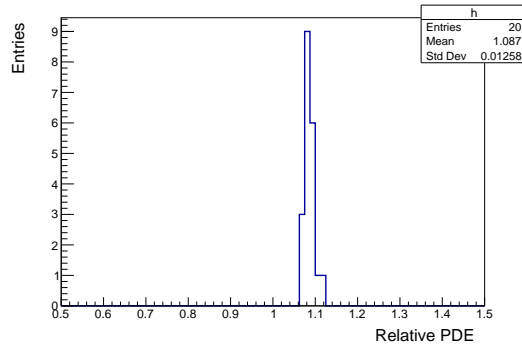
The breakdown voltage is measured five times at ten minutes intervals. Figure 4.14 shows the measurement results of the breakdown voltage. The mean value of the five measurements is 51.91 V and the standard deviation is 0.05 V. The standard deviation is larger than that of the operation voltage. It is caused by the analysis method of the breakdown voltage. As shown in Figure 4.15(a) the breakdown voltage is calculated by the linear extrapolation of the gain-voltage relation. In the process of extrapolation, the variation of the fitting parameters is enlarged. Because the calculated operation voltage is within the range of the measured voltages as shown in 4.15(b), the variation is smaller.

### 4.2.4 Relative PDE

The relative PDE is measured at 55.5 V twenty times at twenty seconds intervals. Figure 4.16 shows the measurement results of the relative PDE. The mean value of the twenty measurements is 1.09 and the standard deviation is 0.01. The ratio of the standard deviation to the mean is

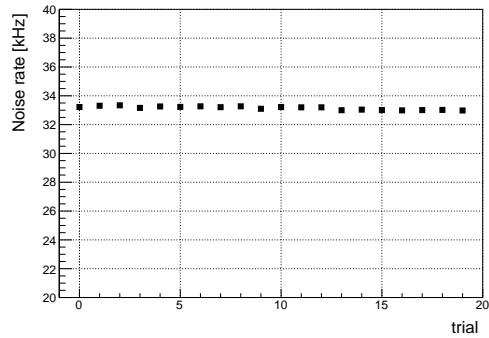


(a) The relative PDE in each measurement.

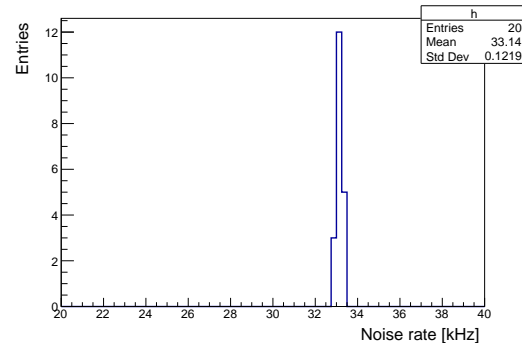


(b) The histogram of the relative PDE.

Figure 4.16: Twenty measurement results of the relative PDE of an MPPC.



(a) The dark noise rate in each measurement.



(b) The histogram of the dark noise rate.

Figure 4.17: Twenty measurement results of the dark noise rate of an MPPC.

1.2% and it satisfies our requirements of 3%.

#### 4.2.5 Dark noise rate

The dark noise rate is measured at 55.5 V twenty times at twenty seconds intervals. Figure 4.17 shows the measurement results of the dark noise rate. The mean value of the twenty measurements is 33.1 kHz and the standard deviation is 0.1 kHz. The ratio of the standard deviation to the mean is 0.4%. The standard deviation is negligible compared to the requirement of 5kHz.

#### 4.2.6 Crosstalk probability

The crosstalk probability is measured five times at 55.5 V at 5 minutes intervals. For each measurement, the threshold scan as described in Section 3.5.6 is performed. Figure 4.18 shows the measurement results of the crosstalk probability. The mean value of the five measurements is 0.87% and the standard deviation is 0.02%. It meets the requirements of 0.1%.

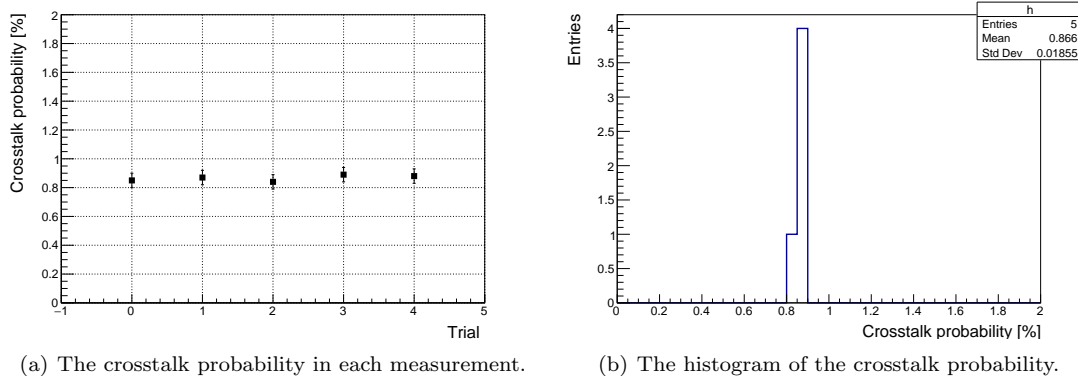


Figure 4.18: Five measurement results of the crosstalk probability of an MPPC.

	Mean	StdDev	StdDev / Mean
Gain	$4.3 \times 10^5$	$0.04 \times 10^5$	0.9%
Breakdown voltage	51.91 V	0.05 V	0.1%
Operation voltage	56.01 V	0.01 V	0.02%
Relative PDE	1.09	0.01	1.2%
Dark noise rate	33.1 kHz	0.1 kHz	0.4%
Crosstalk probability	0.87%	0.02%	2.1%

Table 4.1: The variation of measured values in multiple measurements.

## 4.2.7 Summary

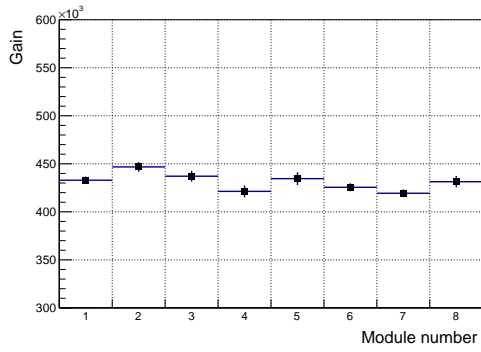
The mean value, standard deviation, and their ratio for each measurement item are summarized in Table 4.1. The variations of all measurement items satisfy the requirements of the test system.

## 4.3 Module dependence of measurement

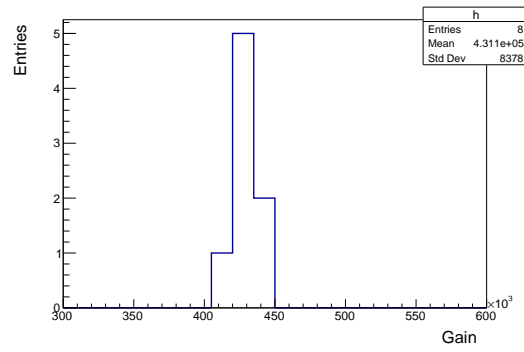
Because we use 512 channels of eight EASIROC modules, measurement results also vary due to the differences in the channels. The possible sources of the differences are, for example, the individual differences of the voltage sources, the amplifiers, and the threshold level. Because it is difficult to correct the differences of all channels, the variations are evaluated as one of the systematic uncertainties of the measurement. To evaluate the typical variations, we measured the gain, operation voltage, breakdown voltage, relative PDE, dark noise rate, and crosstalk probability of the same MPPC on an MPPC-PCB by the corresponding channels in eight different EASIROC modules.

### 4.3.1 Gain

The gain is measured at 55.5 V with eight EASIROC modules. Figure 4.19 shows the measurement results of the gain of an MPPC. The mean value of the measurements by eight EASIROC modules is  $4.3 \times 10^5$  and the standard deviation is  $0.1 \times 10^5$ . The ratio of the standard deviation to the mean is 1.9% and it satisfies the requirement of 3%.

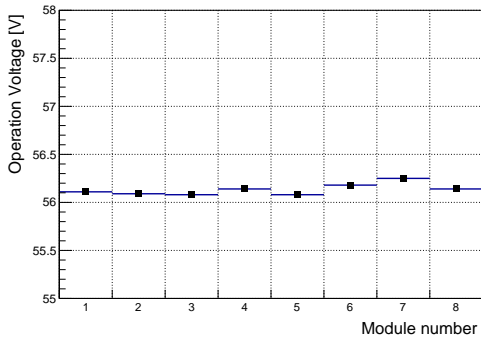


(a) The gain measured by each EASIROC module.

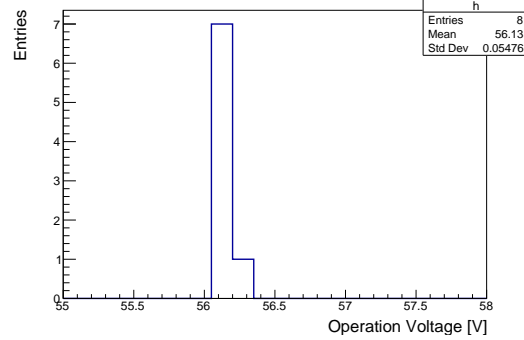


(b) The distribution of the gain.

Figure 4.19: The gain of an MPPC measured by eight EASIROC modules.



(a) The operation voltage measured by each EASIROC module.



(b) The distribution of the operation voltage.

Figure 4.20: The operation voltage of an MPPC when the gain is  $5.0 \times 10^5$  measured by eight EASIROC modules.

### 4.3.2 Operation voltage

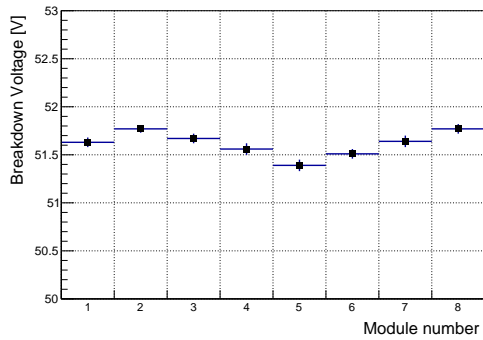
The operation voltage is measured with eight EASIROC modules. Figure 4.20 shows the measurement results of the operation voltage. The mean value of the five measurements is 56.13 V and the standard deviation is 0.05 V. It satisfies the requirement level of 0.1V.

### 4.3.3 Breakdown voltage

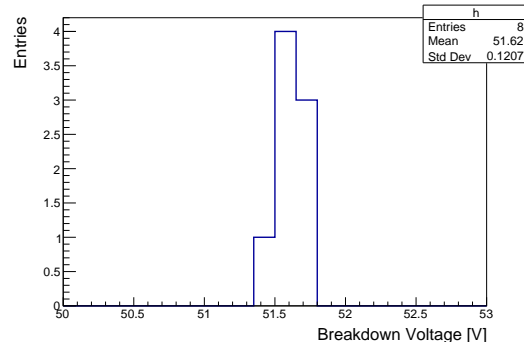
The breakdown voltage is also measured with eight EASIROC modules. Figure 4.21 shows the measurement results of the breakdown voltage. The mean value of the five measurements is 51.62 V and the standard deviation is 0.12 V. Due to the extrapolation process, the variation is larger than that of the operation voltage.

### 4.3.4 Relative PDE

The relative PDE is measured 55.5 V with eight EASIROC modules. Figure 4.22 shows the measurement results of the relative PDE. The mean value of the measurements by eight

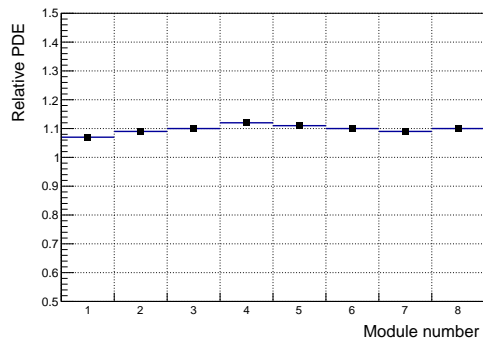


(a) The breakdown voltage measured by each EASIROC module.

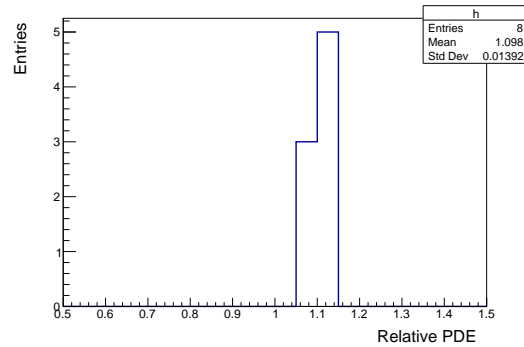


(b) The distribution of the breakdown voltage.

Figure 4.21: The breakdown voltage of an MPPC measured by eight EASIROC modules.



(a) The relative PDE measured by each EASIROC module.



(b) The distribution of the relative PDE.

Figure 4.22: The relative PDE of an MPPC measured by eight EASIROC modules.

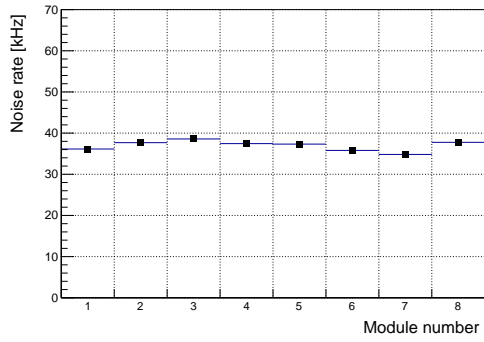
EASIROC modules is 1.10 and the standard deviation is 0.01. The ratio of the standard deviation to the mean is 1.3% and it meets the requirement of 3%.

### 4.3.5 Dark noise rate

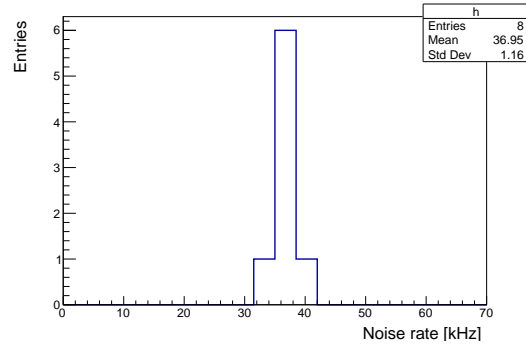
The dark noise rate is measured at 55.5 V with eight EASIROC modules. Figure 4.23 shows the measurement results of the dark noise rate. The mean value of the measurements by eight EASIROC modules is 37.0 kHz and the standard deviation is 1.2 kHz. The variation meets the requirement of 5kHz.

### 4.3.6 Crosstalk probability

The crosstalk probability is measured at 55.5 V with eight EASIROC modules. Figure 4.24 shows the measurement results of the crosstalk probability. The mean value of the measurements by eight EASIROC modules is 0.88% and the standard deviation is 0.05%. The variation satisfies the requirement of 0.1%.

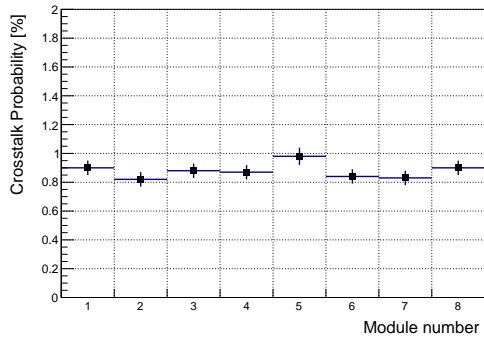


(a) The dark noise rate measured by each EASIROC module.

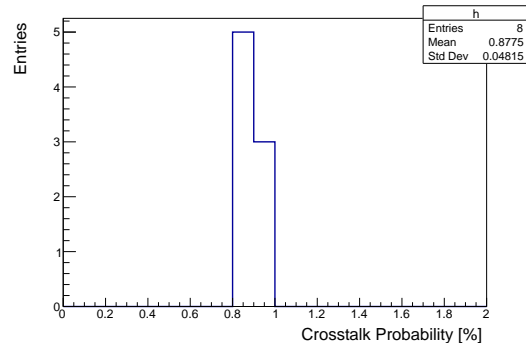


(b) The distribution of the dark noise rate.

Figure 4.23: The dark noise rate of an MPPC measured by eight EASIROC modules.



(a) The crosstalk probability measured by each EASIROC module.



(b) The distribution of the crosstalk probability.

Figure 4.24: The crosstalk probability of an MPPC measured by eight EASIROC modules.

	Mean	StdDev	StdDev / Mean
Gain	$4.3 \times 10^5$	$0.1 \times 10^5$	1.9%
Breakdown voltage	51.62 V	0.12 V	0.3%
Operation voltage	56.13 V	0.05 V	0.1%
Relative PDE	1.10	0.01	1.3%
Dark noise rate	37.0 kHz	1.2 kHz	3.1%
Crosstalk probability	0.88%	0.05%	5.5%

Table 4.2: The variation of the characteristic values measured by eight different EASIROC modules.

### 4.3.7 Summary

The mean value, standard deviation, and their ratio for each measurement item are summarized in Table 4.2. Although the variations are relatively larger than the variations of the stability measurements, they satisfy the requirement level.

## 4.4 Systematic uncertainties of measurement

Based on the measurement results described above, we evaluate the systematic uncertainties of the test system. The systematic uncertainty  $\sigma$  is evaluated as

$$\sigma = \sqrt{\sigma_{\text{stability}}^2 + \sigma_{\text{module}}^2}, \quad (4.1)$$

where  $\sigma_{\text{stability}}$  is the standard deviation of the stability measurements and  $\sigma_{\text{module}}$  is the standard deviation of the module dependence measurements. For the uncertainty of the relative PDE, the effect of the light uniformity  $\sigma_{\text{uniformity}}$  and the effect of the difference of reference MPPCs  $\sigma_{\text{reference}}$  are added as

$$\sigma = \sqrt{\sigma_{\text{stability}}^2 + \sigma_{\text{module}}^2 + \sigma_{\text{uniformity}}^2 + \sigma_{\text{reference}}^2}. \quad (4.2)$$

Table 4.3 summarizes the uncertainties for the measurement items. The requirements for the test system are also written together. The uncertainty for the gain is 2.1% and it is less than the requirement of 3%. The uncertainty for the operation voltage is 0.05 V and it satisfies the requirement. The uncertainty for the breakdown voltage is 0.13 V. It is found that the operation voltage is more precise in evaluating the variation of the voltage behavior of the MPPCs in our analysis method. The uncertainty for the relative PDE is 2.3% and it is less than the requirement of 3%. The uncertainty for the dark noise rate and the crosstalk probability is 1.2 kHz and 0.05% and they are both less than the requirement of 5 kHz and 0.1%, respectively. Therefore, we conclude the precision of the test system is sufficient for assuring the performance of MPPCs used for SuperFGD.

	Uncertainty	Uncertainty (ratio)	Requirement
Gain	$0.1 \times 10^5$	2.1%	< 3% (ratio)
Operation voltage	0.05 V	0.1%	< 0.1 V
Relative PDE	0.02	2.5%	< 3% (ratio)
Dark noise rate	1.2 kHz	3.1%	< 5 kHz
Crosstalk probability	0.05%	5.9%	< 0.1%

Table 4.3: The systematic uncertainty for each measurement item.

# Chapter 5

## Summary and future prospects

### 5.1 Summary

In order to reduce the systematic uncertainty in the T2K experiment, the project of the near detector upgrade is ongoing. As one of the upgrade detectors, a scintillator target detector SuperFGD is newly developed. Because the SuperFGD has high granularity and isotropic structure with three dimensional readouts, it is expected to have the efficient tracking of charged particles and a full polar angle acceptance. These performances will improve the understanding of neutrino-nucleus interactions which are the main sources of the systematic uncertainties for the neutrino oscillation analysis.

The SuperFGD uses 56,384 MPPCs as its photosensors and the uniform and stable operations of those MPPCs are important for the performances of SuperFGD. To test a large number of MPPCs in a reasonable time frame, we have been developing a test system that can measure 512 MPPCs simultaneously. The basic properties of MPPCs such as gain, operation voltage, breakdown voltage, relative PDE, dark noise rate, and crosstalk probability is measured automatically in the test system.

The performance of the test system was evaluated from several points of view. The light uniformity for 64 channels of MPPC-PCB is about 2% level. Although the fluctuation of the light intensity is seen from day to day, such variation is properly corrected by the light intensity measurement of the reference MPPC. The stability and the module dependence of the measurement were also evaluated. The total systematic uncertainties of the test system for gain, operation voltage, breakdown voltage, relative PDE, dark noise rate, and crosstalk probability are 2.1%, 0.05 V, 0.13 V, 2.5%, 1.2 kHz, and 0.05%, respectively, and the precision of the test system is sufficient for the quality assurance purpose of the MPPCs used for SuperFGD.

### 5.2 Future prospects

The test system described in this thesis is still under development. Several tasks need to be completed before we start the performance test. The prospects of future tasks are described in the following sections.

#### 5.2.1 Differences due to light sources and measurement boxes

As discussed in Section 4.1, the combination of a light source and a measurement box satisfies our requirements for light uniformity and stability. We are preparing the other seven light

sources and measurement boxes. The differences due to the use of different light sources and measurement boxes must be checked. Although it is expected that the difference in the light intensity is corrected by the reference MPPCs, if the variation of the relative PDE measurements is larger than our requirement level, a correction will be required.

### **5.2.2 Adjustment of threshold level for each MPPC-PCB**

As discussed in Section 3.4.1, if the threshold level for the dark noise rate measurement is fixed in measurements of all MPPCs, the dark noise rate may be biased due to the difference of gain at the same bias voltage. To avoid such bias, an adjustment of the threshold level for each PCB is needed in the performance test. We are planning a method to adjust the threshold level according to the result of the gain measurement of each PCB which is performed before the dark noise rate measurements.

### **5.2.3 Multiple operation of EASIROCs**

In the test system, eight EASIROC modules are used for the measurements of the MPPC-PCBs and one module is used for the measurements of the reference MPPCs. In the performance test, the nine EASIROC modules are operated in parallel. The method of the multiple operation of the EASIROCs must be established. It will be developed by changing the software program for the operation of EASIROCs.

### **5.2.4 Performance test of the MPPCs used for SuperFGD**

The production of MPPC-PCBs used for SuperFGD will start in April 2021. After the production of the MPPC-PCBs, the performance test of the MPPCs will be conducted by using the developed test system. The estimated test period to measure all MPPC-PCBs is about one month. By the results of the measurements, we will check if each MPPC satisfies our requirements. The measurement results will also be used as a reference after the MPPCs are installed into SuperFGD.

# Acknowledgements

I would like to express my deepest gratitude to my supervisor, Prof. Masashi Yokoyama. He offered many opportunities and practical advice in advancing my research and always encouraged me. I am also deeply grateful to Dr. Kota Nakagiri and Dr. Konosuke Iwamoto for supporting my studies and teaching me a lot of things. I would like to appreciate Dr. Tomohisa Ogawa, Dr. Tsunayuki Matsubara, and Dr. Tatsuya Kikawa for their tremendous cooperation in developing the test system.

I would like to thank Soichiro Kuribayashi, Yuito Awataguchi, Mahesh Jakkapu, Takuji Aihara, Mao Tani, Aoi Eguchi, and Yoshimi Yoshimoto for their collaborative work on SuperFGD and useful advice for my research. I also appreciate the other colleagues in the T2K experiment and T2K Near Detector Upgrade, for the completion of this study. Many thanks go to the members of the Aihara/Yokoyama group, Prof. Hiroaki Aihara, Dr. Yoshiyuki Onuki, Mora Alejandro, Wan Kun, Kohei Matsushita, Shenli Tang, Zhang Tingyu, and Natsumi Ogawa for helpful advice and enjoyable life at the University of Tokyo.

Finally, I would like to express my greatest appreciation to my parents.

# Appendix A

## Measurement results of an MPPC-PCB by eight EASIROCs

As described in Section 4.3, we measure the gain, breakdown voltage, operation voltage, relative PDE, dark noise rate, and crosstalk probability of 64 MPPCs on an MPPC-PCB by using eight EASIROC modules. The gain, relative PDE, dark noise rate, and crosstalk probability are measured at 55.5 V. The distributions of the measured values of 64 MPPCs are shown in Figure A.1~A.6.

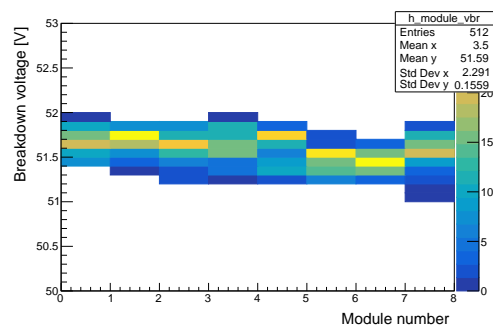
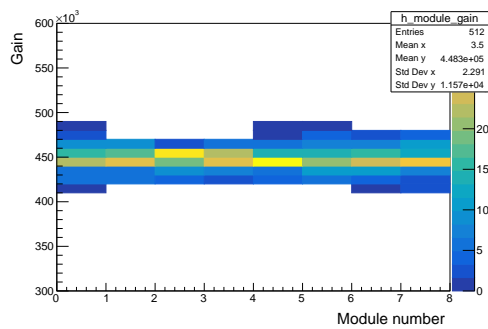


Figure A.1: The distributions of the gain of 64 MPPCs measured by eight EASIROC modules. Figure A.2: The distributions of the breakdown voltage of 64 MPPCs measured by eight EASIROC modules.

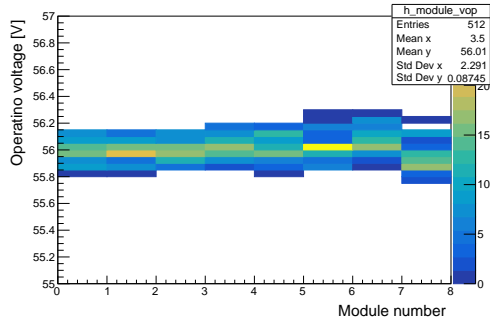


Figure A.3: The distributions of the opera-

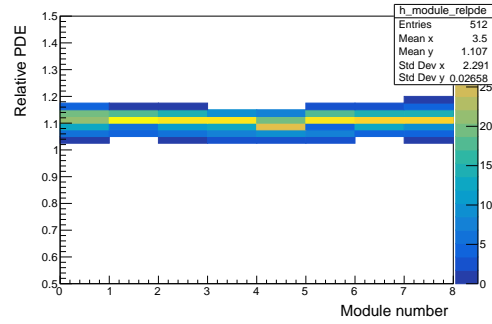


Figure A.4: The distributions of the rela- tive PDE of 64 MPPCs measured by eight EASIROC modules.

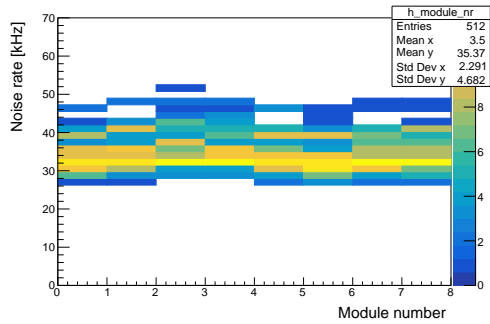


Figure A.5: The distributions of the dark

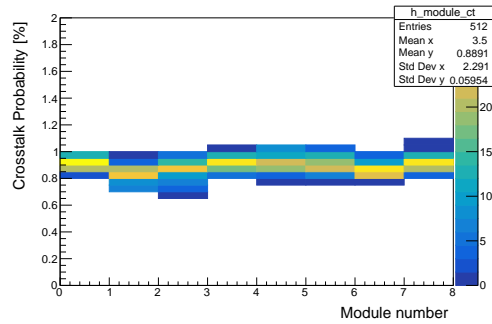


Figure A.6: The distributions of the crosstalk probability of 64 MPPCs measured by eight EASIROC modules.

# List of Figures

1.1	The overview of the T2K experiment. . . . .	5
1.2	The oscillation probability of muon neutrino as a function of energy (top) and the neutrino fluxes for different off-axis angles [6]. . . . .	6
1.3	The ND280 detectors [7]. . . . .	7
1.4	The Super-Kamiokande detector [8]. . . . .	7
1.5	Accumulated POT from Jan 2010 to Feb 2020. . . . .	7
1.6	The structure of an FGD [10]. . . . .	8
1.7	The difficult cases of the reconstruction in the current ND280. . . . .	9
1.8	The design of the ND280 upgrade detector [11]. . . . .	9
1.9	Left : the schematic view of SuperFGD [11]. Right : a scintillator cube with three WLS fibers inserted. . . . .	10
1.10	The advantage of the upgrade detectors in the reconstruction of particles with high angle and low momentum. . . . .	11
1.11	The selection efficiency for muon as a function of the muon polar angle [12]. The purple line shows the efficiency for the current ND280. The blue and green lines show the efficiency for the upgrade configuration. The blue one shows the efficiency for events in which a muon is reconstructed in a TPC. The green one shows the efficiency for events in which a muon stops and is reconstructed in SuperFGD in addition to the events in TPC. . . . .	11
1.12	Track reconstruction efficiency for protons stopping in SuperFGD (red line) and FGD (black dashed line) [12]. . . . .	12
1.13	Average energy deposit per unit length for a sample of a mix of muons and pions (red) and a sample of protons (blue) [13]. . . . .	13
2.1	The operation principle of photodiode [15]. . . . .	15
2.2	Schematic diagram of avalanche multiplication [15]. . . . .	15
2.3	The operation process of a combination of the Geiger mode APD and the quenching resistor. . . . .	16
2.4	The operating principle of the MPPC [15]. . . . .	17
2.5	Left:picture of the MPPC S13360-1325PE. Right:dimensional specifications of S13360-1325PE [17]. . . . .	19
2.6	Pictures of MPPC-PCB prototype. . . . .	20
2.7	Reel package of MPPC. . . . .	21
2.8	Operation voltage measured by Hamamatsu. . . . .	22
2.9	Mean light yield produced by minimum ionizing particles for 384 readout channels of the prototype of SuperFGD [13]. Each line shows light yield calculated by a different calibration method. The variation is about $\pm 25\%$ at maximum in all methods. . . . .	23

2.10	The distribution of the gain and the relative PDE of S13360 MPPCs used in another near detector of T2K experiment [18]. . . . .	23
3.1	Schematic view of the MPPC test system. . . . .	27
3.2	The front side of the NIM EASIROC board. . . . .	28
3.3	The block diagram of an EASIROC chip [24]. . . . .	28
3.4	Light source used in the test system. . . . .	29
3.5	Wavelength dependence of PDE of MPPC S13360-1325PE (black line). The blue line shows LED's peak wavelength. The green line shows the peak emission wavelength of WLS fiber. . . . .	30
3.6	The reference MPPC. . . . .	31
3.7	The measurement box. . . . .	31
3.8	The readout cable. . . . .	32
3.9	The interface board. . . . .	32
3.10	The thermostatic chambers. . . . .	33
3.11	Threshold curve . . . . .	34
3.12	The histogram of measured 0.5 p.e. level threshold DAC for each EASIROC chip of an EASIROC module. . . . .	35
3.13	Hold time scan. The plot is fitted by a quadratic function (red line). . . . .	36
3.14	The histogram of the measured peak timings for all 64 channels of an EASIROC module. . . . .	37
3.15	The circuit of calibration pulse injection. . . . .	37
3.16	Relation between ADC and injected charge. . . . .	37
3.17	The conversion factors for 64 channels of eight EASIROC modules. . . . .	38
3.18	The pulse height and the gain of an MPPC measured by eight EASIROC modules. . . . .	38
3.19	The gain measurement. . . . .	41
3.20	The breakdown voltage and overvoltage measurement. . . . .	41
3.21	Overvoltage dependence of the number of detected photons and the relative PDE. . . . .	43
3.22	The dark noise rate measurement. . . . .	43
3.23	The crosstalk probability measurement. . . . .	44
4.1	A prototype of measurement box. . . . .	46
4.2	The distribution of the light intensity measured in a prototype of the measurement box . . . . .	46
4.3	The measurement box with mirror sheet. . . . .	46
4.4	The distribution of the light intensity measured with the mirror sheet. . . . .	47
4.5	The measurement setup for testing dependence of the light uniformity on the positions of the light sources. . . . .	47
4.6	The relation between the light uniformity and the position of the diffuser. . . . .	48
4.7	The distribution of the light intensity measured in the final design box. . . . .	48
4.8	The result of the light stability measurement in a short period of time. . . . .	49
4.9	The result of the light stability measurement in a middle period of time. . . . .	49
4.10	The measurement of relative PDE. . . . .	50
4.11	Twenty measurement results of the gain of an MPPC. . . . .	51
4.12	The result of the gain measurement in a middle period of time. . . . .	51
4.13	Five measurement results of the operation voltage when the gain is $5.0 \times 10^5$ of an MPPC. . . . .	51
4.14	Five measurement results of the breakdown voltage of an MPPC. . . . .	52

4.15	The analysis method of the breakdown voltage and the operation voltage when the gain is $5.0 \times 10^5$ . . . . .	52
4.16	Twenty measurement results of the relative PDE of an MPPC. . . . .	53
4.17	Twenty measurement results of the dark noise rate of an MPPC. . . . .	53
4.18	Five measurement results of the crosstalk probability of an MPPC. . . . .	54
4.19	The gain of an MPPC measured by eight EASIROC modules. . . . .	55
4.20	The operation voltage of an MPPC when the gain is $5.0 \times 10^5$ measured by eight EASIROC modules. . . . .	55
4.21	The breakdown voltage of an MPPC measured by eight EASIROC modules. . . . .	56
4.22	The relative PDE of an MPPC measured by eight EASIROC modules. . . . .	56
4.23	The dark noise rate of an MPPC measured by eight EASIROC modules. . . . .	57
4.24	The crosstalk probability of an MPPC measured by eight EASIROC modules. . . . .	57
A.1	The distributions of the gain of 64 MPPCs measured by eight EASIROC modules. . . . .	63
A.2	The distributions of the breakdown voltage of 64 MPPCs measured by eight EASIROC modules. . . . .	63
A.3	The distributions of the operation voltage of 64 MPPCs measured by eight EASIROC modules. . . . .	64
A.4	The distributions of the relative PDE of 64 MPPCs measured by eight EASIROC modules. . . . .	64
A.5	The distributions of the dark noise rate of 64 MPPCs measured by eight EASIROC modules. . . . .	64
A.6	The distributions of the crosstalk probability of 64 MPPCs measured by eight EASIROC modules. . . . .	64

# List of Tables

2.1	Comparison of photo sensors. . . . .	16
2.2	Specifications of the S13360-1325PE. The characteristics are measured at $V_{\text{over}} = 5$ V and 25 °C . . . . .	20
2.3	The requirements for the basic properties of MPPCs used in SuperFGD. . . . .	24
3.1	The requirements for measurement uncertainties of the test system. . . . .	26
3.2	Specification of the S13081-050CS MPPC used as the reference MPPCs. . . . .	30
3.3	The 0.5 p.e. level threshold DAC for 16 EASIROC chips. The values are decided by the measurements of an MPPC-PCB. . . . .	35
3.4	Measurement mode for the performance test. . . . .	39
3.5	The relative PDE of the reference MPPCs to a standard MPPC . . . . .	42
4.1	The variation of measured values in multiple measurements. . . . .	54
4.2	The variation of the characteristic values measured by eight different EASIROC modules. . . . .	58
4.3	The systematic uncertainty for each measurement item. . . . .	59

# Bibliography

- [1] A.D. Sakharov. Violation of CP Invariance, C asymmetry, and baryon asymmetry of the universe. *Sov. Phys. Usp.*, 34(5):392–393, 1991.
- [2] M. Fukugita and T. Yanagida. Baryogenesis Without Grand Unification. *Phys. Lett. B*, 174:45–47, 1986.
- [3] Y. Fukuda et al. Evidence for Oscillation of Atmospheric Neutrinos. *Phys. Rev. Lett.*, 81:1562–1567, Aug 1998.
- [4] Ziro Maki, Masami Nakagawa, and Shoichi Sakata. Remarks on the Unified Model of Elementary Particles. *Progress of Theoretical Physics*, 28(5):870–880, 11 1962.
- [5] B. Pontecorvo. Neutrino Experiments and the Problem of Conservation of Leptonic Charge. *Sov. Phys. JETP*, 26:984–988, 1968.
- [6] K. Abe et al. T2K neutrino flux prediction. *Phys. Rev. D*, 87:012001, Jan 2013.
- [7] K. Abe et al. The T2K Experiment. *Nucl. Instrum. Meth. A*, 659:106–135, 2011.
- [8] Super-Kamiokande detector. <https://www.ipmu.jp/en/node/1655>.
- [9] K. Abe et al. Constraint on the matter–antimatter symmetry-violating phase in neutrino oscillations. *Nature*, 580(7803):339–344, 2020.
- [10] K.Ieki. *Observation of  $\nu_\mu \rightarrow \nu_e$  oscillation in the T2K experiment*. PhD thesis, Kyoto University, Japan, 2014.
- [11] K. Abe et al. T2K ND280 Upgrade - Technical Design Report. *CERN-SPSC-2019-001 (SPSC-TDR-006)*, 2019.
- [12] D.Sgalaberna. The T2K ND280 upgrade. [https://indico.cern.ch/event/868940/contributions/3817023/attachments/2081306/3495881/ND280\\_upgrade\\_ICHEP2020\\_-\\_final.pdf](https://indico.cern.ch/event/868940/contributions/3817023/attachments/2081306/3495881/ND280_upgrade_ICHEP2020_-_final.pdf). ICHEP 2020.
- [13] A. Blondel et al. The SuperFGD Prototype charged particle beam tests. *Journal of Instrumentation*, 15(12):P12003–P12003, dec 2020.
- [14] Hamamatsu Photonics K.K. *Product information Hamamatsu*, 2020.
- [15] Hamamatsu Photonics K.K. *Opto-semiconductor 2014*, 2014.
- [16] Tsunayuki Matsubara. Application of MPPC for T2K near Detector Upgrade. In *Proceedings of the 5th International Workshop on New Photon-Detectors (PD18)*.

- [17] Hamamatsu Photonics K.K. *S13360series, MPPCs for precision measurement.*
- [18] R.Tamura. Construction and performance of a neutrino detector for neutrino-nucleus interaction cross-section measurements. Master's thesis, The university of tokyo, Japan, 2018.
- [19] M. Yokoyama et al. Performance of multi-pixel photon counters for the T2K near detectors. *Nuclear Instruments and Methods in Physics Research Section A: Accelerators, Spectrometers, Detectors and Associated Equipment*, 622(3):567 – 573, 2010.
- [20] F. Moreau et al. Mass characterization of multi-pixel photon counters for the T2K 280m near detector. *Nuclear Instruments and Methods in Physics Research Section A: Accelerators, Spectrometers, Detectors and Associated Equipment*, 613(1):46 – 53, 2010.
- [21] A. Vacheret et al. Characterization and simulation of the response of Multi-Pixel Photon Counters to low light levels. *Nuclear Instruments and Methods in Physics Research Section A: Accelerators, Spectrometers, Detectors and Associated Equipment*, 656(1):69 – 83, 2011.
- [22] F.Hosomi. Characterization of Multi-Pixel Photon Counters for a new neutrino detector. Master's thesis, The university of tokyo, Japan, 2016.
- [23] R. Honda et al. The development of the multi PPD readout electronics with EASIROC and SiTCP. *PoS, PhotoDet2012:031*, 2012.
- [24] Omega. *EASIROC DATASHEET*, 2011.
- [25] Nichia Corporation. *SPECIFICATIONS FOR BLUE LED*, 2020.